ELSEVIER

Bacterial gene regulation in diauxic and non-diauxic growth

Atul Narang[a],*, Sergei S. Pilyugin[b]

[a]Department of Chemical Engineering, University of Florida, Gainesville, FL 32611-6005, USA
[b]Department of Mathematics, University of Florida, Gainesville, FL 32611-8105, USA

Abstract

When bacteria are grown in a batch culture containing a mixture of two growth-limiting substrates, they exhibit a rich spectrum of substrate consumption patterns including diauxic growth, simultaneous consumption, and bistable growth. In previous work, we showed that a minimal model accounting only for enzyme induction and dilution captures all the substrate consumption patterns [Narang, A., 1998a. The dynamical analogy between microbial growth on mixtures of substrates and population growth of competing species. Biotechnol. Bioeng. 59, 116–121, Narang, A., 2006. Comparitive analysis of some models of gene regulation in mixed-substrate microbial growth, J. Theor. Biol. 242, 489–501]. In this work, we construct the bifurcation diagram of the minimal model, which shows the substrate consumption pattern at any given set of parameter values. The bifurcation diagram explains several general properties of mixed-substrate growth. (1) In almost all the cases of diauxic growth, the ''preferred'' substrate is the one that, by itself, supports a higher specific growth rate. In the literature, this property is often attributed to the optimality of regulatory mechanisms. Here, we show that the minimal model, which accounts for induction and growth only, displays the property under fairly general conditions. This suggests that the higher growth rate of the preferred substrate is an intrinsic property of the induction and dilution kinetics. It can be explained mechanistically without appealing to optimality principles. (2) The model explains the phenotypes of various mutants containing lesions in the regions encoding for the operator, repressor, and peripheral enzymes. A particularly striking phenotype is the ''reversal of the diauxie'' in which the wild-type and mutant strains consume the very same two substrates in opposite order. This phenotype is difficult to explain in terms of molecular mechanisms, such as inducer exclusion or CAP activation, but it turns out to be a natural consequence of the model. We show furthermore that the model is robust. The key property of the model, namely, the competitive dynamics of the enzymes, is preserved even if the model is modified to account for various regulatory mechanisms. Finally, the model has important implications for the problem of size regulation in development. It suggests that protein dilution may be the mechanism coupling patterning and growth.
© 2006 Elsevier Ltd. All rights reserved.

Keywords: Mathematical model; Gene regulation; Mixed substrate growth; Substitutable substrates; Lac operon; Lotka–Volterra model

1. Introduction

When microbial cells are grown in a batch culture containing a mixture of two carbon sources, they often exhibit *diauxic* growth (Monod, 1947). This phenomenon is characterized by the appearance of two exponential growth phases separated by a lag phase called *diauxic lag*. The most well-known example of the diauxie is the growth of *Escherichia coli* on a mixture of glucose and lactose. Early studies by Monod showed that in this case, the two exponential growth phases reflect the sequential consumption of glucose and lactose (Monod, 1942). Moreover, only glucose is consumed in the first exponential growth phase because the synthesis of the *peripheral* enzymes for lactose is somehow abolished in the presence of glucose. These enzymes include lactose permease (which catalyses the transport of lactose into the cell), β-galactosidase (which hydrolyses the intracellular lactose into products that feed into the glycolytic pathway) and lactose transacetylase (which is believed to metabolize toxic thiogalactosides transported by lactose permease). During the period of preferential growth on glucose, the peripheral enzymes for

---

*Corresponding author. Tel.: +1 352 392 0028; fax: +1 352 392 9513.
E-mail address: narang@che.ufl.edu (A. Narang).
URL: http://narang.che.ufl.edu.

lactose are diluted to very small levels. The diauxic lag reflects the time required to build up these enzymes to sufficiently high levels. After the diauxic lag, one observes the second exponential phase corresponding to consumption of lactose.

It turns out that the peripheral enzymes for lactose are synthesized only if lactose is present in the environment. The mechanism for the synthesis or *induction* of these enzymes in the presence of lactose and absence of glucose was discovered by Monod and coworkers (Jacob and Monod, 1961). It was shown that the genes corresponding to these enzymes are contiguous on the DNA and transcribed in tandem, an arrangement referred to as the *lac* operon Fig. 1(a). In the absence of lactose, the *lac* operon is not transcribed because a molecule called the *lac* repressor is bound to a specific site on the *lac* operon called the *operator* (Fig. 1b, bottom). This prevents RNA polymerase from attaching to the operon and initiating transcription. In the presence of lactose, transcription of
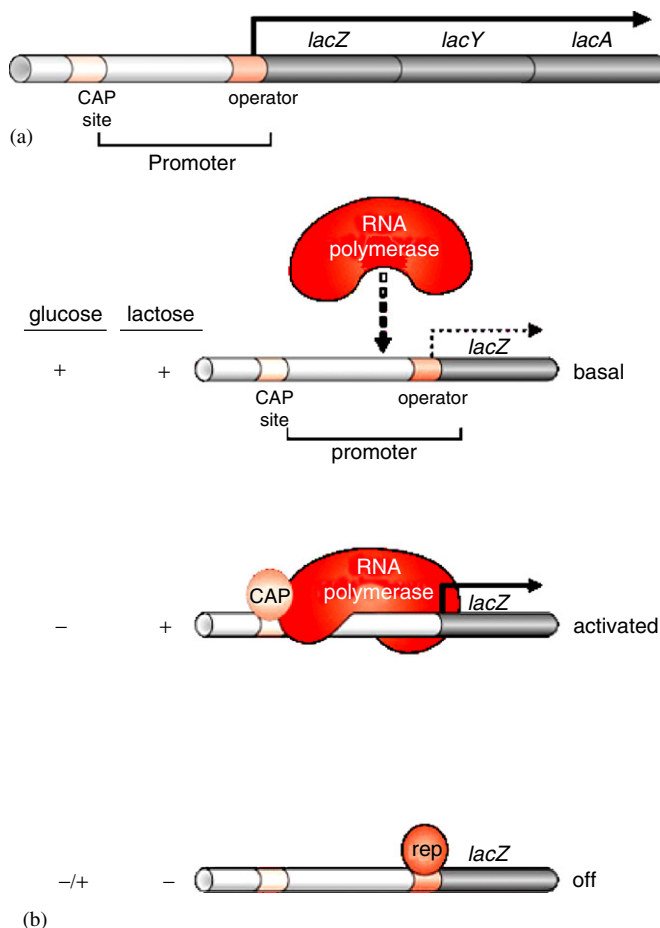

(a)

(b)

Fig. 1. Molecular mechanism for induction and repression of the *lac* operon in *E. coli* (Ptashne and Gann, 2002): (a) Structure of the *lac* operon. The *lacZ*, *lacY*, and *lacA* genes code for β-galactosidase, lactose permease, and lactose transacetylase, respectively. The *operator, promoter,* and *CAP site* denote the DNA sequences which bind the repressor, RNA polymerase, and CAP-cAMP, respectively. (b) The states of the *lac* operon in the presence of glucose or/and lactose. The repressor and CAP-cAMP complex are denoted *rep* and *CAP*, respectively.

lac is triggered because allolactose, a product of β-galactosidase, binds to the repressor, and renders it incapable of binding to the operator (Fig. 1b, middle).[1]

The occurrence of the glucose–lactose diauxie suggests that transcription of *lac* is somehow repressed in the presence of glucose. Two molecular mechanisms have been proposed to explain this repression:

(1) *Inducer exclusion* (Postma et al., 1993): In the presence of glucose, enzyme IIA^{glc}, a peripheral enzyme for glucose, is dephosphorylated. The dephosphorylated IIA^{glc} inhibits lactose uptake by binding to lactose permease. This reduces the intracellular concentration of allolactose, and hence, the transcription rate of the *lac* operon.

Genetic evidence suggests that phosphorylated IIA^{glc} activates the enzyme, adenylate cyclase, which catalyses the synthesis of cyclic AMP (cAMP). Since the total concentration of IIA^{glc} remains constant on the rapid time scale of its dephosphorylation, exposure of the cells to glucose causes a decrease in the level of phosphorylated IIA^{glc}, and hence, cAMP. This reduction of the cAMP level forms the basis of yet another mechanism of *lac* repression.

(2) *cAMP activation* (Ptashne and Gann, 2002, Chapter 1): It has been observed that RNA polymerase is not recruited to the *lac* operon unless a protein called catabolite activator protein (CAP) or cAMP receptor protein (CRP) is bound to a specific site on the *lac* operon (denoted "CAP site" in Fig. 1). Furthermore, CAP, by itself, has a low affinity for the CAP site, but when bound to cAMP, its affinity for the CAP site increases dramatically. The inhibition of *lac* transcription by glucose is then explained as follows.

In the presence of lactose alone (i.e. no glucose), the cAMP level is high. Hence, CAP becomes cAMP-bound, attaches to the CAP site, and promotes transcription by recruiting RNA polymerase (Fig. 1b, middle). When glucose is added to the culture, the cAMP level decreases by the mechanism described above. Consequently, CAP, being cAMP-free, fails to bind to the CAP site, and *lac* transcription is abolished (Fig. 1b, top).

We show below that neither one of these two mechanisms can fully explain the glucose-mediated repression of *lac* transcription.

The following three observations contradict the cAMP activation model.

(1) The intracellular cAMP levels during the first exponential growth phase (~2.5 μM) are comparable, if not higher, than those observed during the second exponential growth phase (~1.25 − 2 μM) (see Fig. 2(a)).

---

[1] A similar mechanism serves to induce the genes for glucose transport (Plumbridge, 2003, Fig. 4).
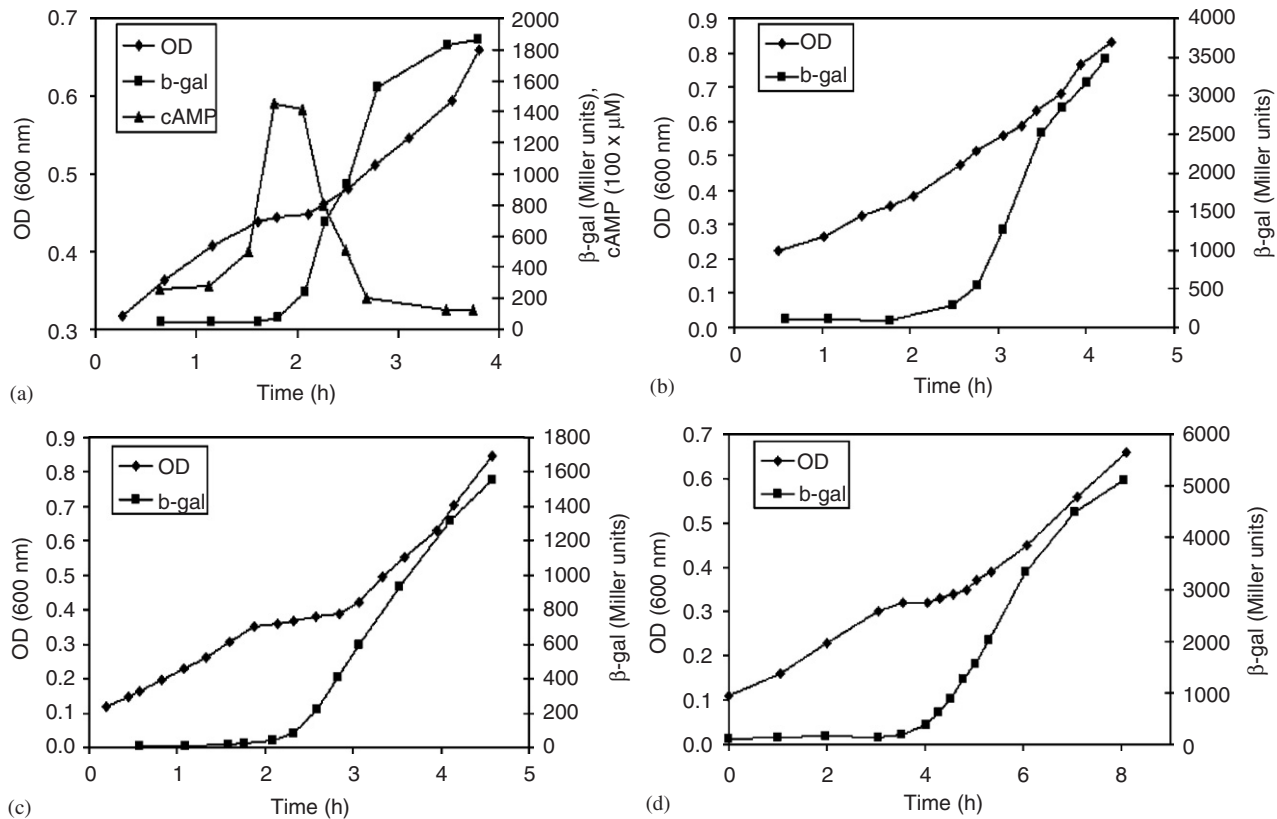
Fig. 2. Repression of *lac* transcription in the presence of glucose is not due to reduced cAMP levels (Inada et al., 1996; Kimata et al., 1997). OD denotes optical density, and Miller units are a measure of *β*-galactosidase activity. (a) Growth of the wild-type strain, *E. coli* W3110, on glucose + lactose. The intracellular cAMP levels are comparable during the two exponential growth phases. (b) Growth of *E. coli* W3110 on glucose + lactose in the presence of 5 mM cAMP. Despite the high cAMP concentration, *β*-galactosidase synthesis is repressed during the first exponential growth phase. (c, d) Growth of *E. coli* △*cya crp*** and PR166 on glucose + lactose. The *lac* transcription rate in these strains is independent of the cAMP level, but *β*-galactosidase synthesis is repressed during the first exponential growth phase.

It follows that the repression of *lac* transcription in the presence of glucose is not due to lower cAMP levels.[2]

(2) When the culture is exposed to large concentrations (5 mM) of exogenous cAMP, the diauxic lag vanishes, but the *lac* operon still fails to be transcribed during the first exponential growth phase (Fig. 2b).

The disappearance of the diauxic lag implies that an elevated level of intracellular cAMP does stimulate the *lac* transcription rate. However, it fails to relieve the repression of *lac* transcription in the presence of glucose.

(3) Diauxic growth persists in cells which transcribe the *lac* operon at a rate that is independent of cAMP levels. This has been demonstrated with two types of cells (Fig. 2c,d). In *E. coli* △*cya crp** mutants, *crp*, the gene coding for CAP, is mutated such that CAP binds to the CAP site even in the absence of cAMP. In *E. coli* PR166, the *lac* promoter is mutated such that RNA polymerase binds to the promoter even if there is no

CAP-cAMP at the CAP site. In both cases, transcription of *lac* is independent of cAMP levels. Yet, *β*-galactosidase synthesis is still repressed during the first exponential growth phase.

These results show that higher cAMP levels do stimulate the *lac* transcription rate. Indeed, the 5-fold increase in cAMP levels at the end of the first exponential growth phase in Fig. 2a is characteristic of cells exposed to low concentrations (0.3 mM) of glucose (Notley-McRobb et al., 1997), and it is likely that this serves to reduce the length of the diauxic lag. However, *lac* transcription is repressed in the presence of glucose even if the ability of cAMP to influence *lac* transcription is abolished.

The persistence of the glucose–lactose diauxie in cAMP-independent cells has led to the hypothesis that inducer exclusion alone is responsible for inhibiting *lac* transcription (Inada et al., 1996; Kimata et al., 1997). However, inducer exclusion exerts a relatively mild effect on lactose uptake. In *E. coli* ML30, the activity of lactose permease is inhibited no more than ∼40% at saturating concentrations of glucose (Cohn and Horibata, 1959, Table 2). This *partial* inhibition by inducer exclusion cannot explain the *almost complete* inhibition of *lac* transcription.

---

[2]Excess cAMP fails to relieve the repression of transcription during growth of *E. coli* on other pairs of substrates, such as glucose + melibiose (Okada et al., 1981, Fig. 4) and glucose + galactose (see Fig. 9a of this work).

Thus, despite several decades of research, no molecular mechanism has been found to fully explain the glucose–lactose diauxie in *E. coli*. It is therefore particularly striking that the minimal model described below predicts diauxic growth, despite the absence of inducer exclusion and cAMP activation.

In the meantime, microbial physiologists have accumulated a vast body of work showing that diauxic growth is ubiquitous. It has been observed in diverse microbial species on many pairs of *substitutable* substrates (i.e. substrates that satisfy the same nutrient requirements) including pairs of carbon sources (Egli, 1995; Harder and Dijkhuizen, 1982; Kovarova-Kovar and Egli, 1998), nitrogen sources (Neidhardt and Magasanik, 1957), phosphorus sources (Daughton et al., 1979), and electron acceptors (Liu et al., 1998). These studies show that there is no correlation between the chemical identity of a compound and its ability to act as the preferred substrate. For instance, during growth on a mixture of glucose and an organic acid, enteric bacteria, such as *E. coli*, prefer glucose, whereas soil bacteria, such as *Pseudomonas* and *Arthrobacter*, prefer the organic acid (Harder and Dijkhuizen, 1976, 1982). However, there is a correlation between the maximum specific growth rate on a compound and its ability to act as a preferred substrate.

> In most cases, although not invariably, the presence of a substrate permitting a higher growth rate prevents the utilization of a second, 'poorer', substrate in batch culture (Harder and Dijkhuizen, 1982, p. 461).

This remarkable correlation, which is reminiscent of anthropomorphic choice, is often rationalized by appealing to teleological (design-oriented) arguments. Harder and Dijkhuizen assert, for instance, that consumption of lactose is abolished in the presence of glucose because this prevents "unnecessary synthesis of catabolic enzymes in cells that already have available a carbon and energy source that allows fast growth" (Harder and Dijkhuizen, 1982, p. 463). However, there is no mechanistic explanation for this correlation.

Although the diauxie dominates the literature on mixed-substrate growth, there is ample evidence of non-diauxic growth. In *E. coli* K12, several pairs of organic acids are consumed simultaneously (Narang et al., 1997b), one example of which is shown in Fig. 3a. The maximum specific growth rates on these organic acids are in the range $0.28 - 0.44\,\mathrm{h}^{-1}$, which are low compared to the largest maximum specific growth rate sustained in a minimal (synthetic) medium ($0.74\,\mathrm{h}^{-1}$ on glucose). Similar behavior has been observed in other species, leading Egli to conclude that

> Especially combinations of substrates that support medium or low maximum specific growth rates are utilized simultaneously (Egli, 1995, p. 325).

However, a closer look at data suggests that low or medium growth rates are not necessary for simultaneous consumption. This is evident from Monod's early studies with the so-called "A-sugars," namely, glucose, fructose, mannitol, mannose, and sucrose (Monod, 1942, 1947).[3] He found that in *E. coli* and *B. subtilis*, these sugars supported comparable maximum specific growth rates, but there was no diauxic lag during growth on a mixture of glucose and any one of the other A-sugars. Subsequent studies have confirmed that in some of these cases, both the substrates are consumed simultaneously (Fig. 3b). Now, in all the cases of simultaneous consumption described above, the single-substrate growth rates were comparable. Thus, it is conceivable that simultaneous consumption occurs whenever the *ratio* of the single-substrate growth rates is close to 1. It turns out that this condition may be necessary, but it is certainly not sufficient. Although the growth rates of *Propionibacterium shermanii* on glucose and lactate are identical (0.141 and $0.142\,\mathrm{h}^{-1}$, respectively), lactate is consumed preferentially (Lee et al., 1974). Similarly, the growth rates of *E. coli* ML308 on glucose and fructose are comparable (0.91 and $0.73\,\mathrm{h}^{-1}$, respectively), but glucose is consumed preferentially (Clark and Holms, 1976).[4] Thus, current evidence suggests that the existence of comparable single-substrate growth rates is, perhaps, necessary, but not sufficient, for simultaneous consumption. It seems desirable to understand the mechanistic basis of this observation.

In addition to simultaneous substrate utilization, there is some evidence that the substrate utilization pattern can depend on the history of the preculture. Hamilton and Dawes were among the first to observe such behavior during the growth of *Pseudomonas aeruginosa* on a mixture of citrate and glucose (Hamilton and Dawes, 1959, 1960, 1961). Cells precultured on citrate showed diauxic growth with citrate as the preferred substrate, whereas cells precultured on glucose consumed both citrate and glucose. We observed a similar substrate consumption pattern during growth of *E. coli* K12 on glucose and pyruvate (Narang et al., 1997b). An entirely different preculture-dependent pattern was obtained during the growth of a pseudomonad on glucose and phenol (Panikov, 1995, Chapter 3, p. 181). When the cells were precultured on glucose, there was preferential consumption of glucose. Immediately after the exhaustion of phenol, when the cells were fully adapted to phenol, the medium was supplemented with additional glucose and phenol. Once again, there was diauxic growth, but phenol, rather than glucose, was the preferred substrate. In earlier work, we have argued that preculture-dependent growth patterns may be quite common—the lack of such data reflects the fact that the

---

[3]It was found later that all the A-sugars are transported by the phosphotransferase system (PTS) (Roseman and Meadow, 1990).

[4]The absence of the diauxic lag, observed in Monod's earlier studies with glucose–fructose mixtures, is due to rapid de novo synthesis of the PTS enzymes for fructose (Clark and Holms, 1976, Figs. 4 and 5). Thus, preferential consumption without a lag does not imply the existence of new molecular mechanisms—it can be a consequence of rapid induction kinetics.
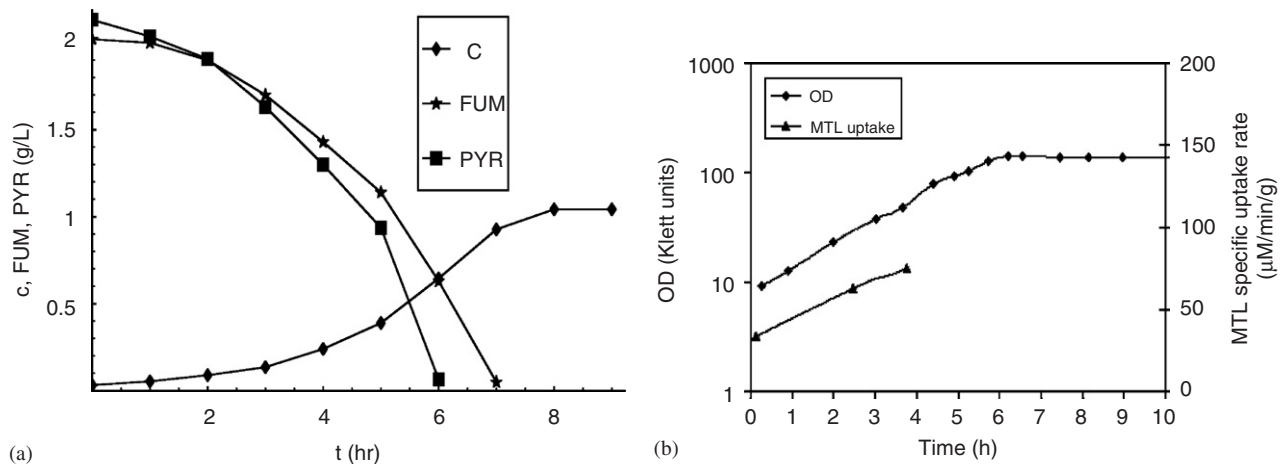
Fig. 3. Simultaneous consumption of substrates in batch cultures: (a) simultaneous consumption of fumarate (FUM) and pyruvate (PYR) during batch growth of *E. coli* K12 (*c* denotes the cell density in gms dry weight per liter). The single-substrate maximum specific growth rates on fumarate and pyruvate are 0.41 and 0.28 h^{-1}, respectively. This growth pattern is observed with several pairs of organic acids (Narang et al., 1997b). (b) Simultaneous consumption of glucose and mannitol (MTL) during batch growth of *E. coli* strain 158 (Lengeler and Lin, 1972). There is significant uptake of mannitol during the first 4 h even though the cells are precultured on glucose.

effect of preculturing was not investigated in most studies (Narang et al., 1997b). In order to facilitate their identification, it seems appropriate to determine the feasible preculture-dependent growth patterns.

The goal of this work is to seek mechanistic answers for the following questions:

(1) In diauxic growth, why is the maximum specific growth rate on the preferred substrate higher than that on the less preferred substrate?
(2) Under what conditions are the substrates consumed simultaneously?
(3) What types of preculture-dependent growth patterns are feasible?

There are numerous mechanistic models of mixed-substrate growth. Many of them are based on detailed mechanisms uniquely associated with the glucose–lactose diauxie in *E. coli* (Kremling et al., 2001; Santillan and Mackey, 2004; van Dedem and Moo-Young, 1973; Wong et al., 1997). These models cannot address the above questions, which are concerned with the *general* properties of mixed-substrate growth. Thus, one led to consider the more general models accounting for only those processes that are common to most systems of mixed-substrate growth (Brandt et al., 2004; Narang et al., 1997a; Narang, 1998a; Thattai and Shraiman, 2003). Recently, we have shown that these general models are similar inasmuch as the enzymes follow competitive dynamics in all the cases (Narang, 2006). However, the model in Brandt et al. cannot capture non-diauxic growth, and the model in Thattai and Shraiman treats the specific growth rate as a fixed (constant) parameter, an assumption that is not appropriate for describing the growth of batch cultures.

In this work, we address the questions posed above by appealing to the minimal model in Narang (1998a). This

model accounts for only enzyme induction and dilution, the two processes that occur in almost all systems of mixed-substrate growth. Yet, it captures all the batch growth patterns described above, and its extension to continuous cultures predicts all the steady states observed in chemostats (Narang, 1998b). Here, we show that the minimal model also provides mechanistic explanations for the foregoing questions. Specifically, we find that

(1) if the induction kinetics are hyperbolic, the maximum specific growth rate on the preferred substrate is always higher than that on the less preferred substrate. The manifestation of this correlation in a minimal model containing only enzyme induction and dilution suggests that its existence is not due to goal-oriented regulatory mechanisms, an assumption that lies at the heart of models based on optimality principles (Mahadevan et al., 2002; Kompala et al., 1986; Ramakrishna et al., 1996). It is an intrinsic property resulting from the kinetics of enzyme induction and dilution. We also find that the correlation can be violated when the induction kinetics are sigmoidal, and that the dynamics of these offending cases are consistent with the data in the literature.
(2) the existence of comparable single-substrate growth rates is not sufficient for simultaneous consumption. This agrees with the data described above. However, we find that this condition is not necessary either. This is because the occurrence of simultaneous consumption depends not only on the relative growth rates, but also on the saturation constants for induction. If these saturation constants are small, there is simultaneous consumption, regardless of the relative growth rates.

We show, furthermore, that the classification of the substrate consumption patterns predicted by the model

explains the phenotypes of several mutants. The most striking phenotype is the *reversal of the diauxie*, wherein both the wild-type and the mutant strains display diauxic growth, but consume the substrates in opposite order. This phenotype cannot be explained in terms of the standard molecular mechanisms, but turns out to be a natural consequence of the minimal model.

2. The model

Fig. 4 shows the kinetic scheme of the minimal model. Here, S_i denotes the ith exogenous substrate, E_i denotes the transport enzyme for S_i, X_i denotes internalized S_i, and C^- denotes *all* intracellular components except E_i and X_i (thus, it includes precursors, free amino acids, and macromolecules).

In this work, attention will be confined to growth in batch cultures. We assume that

(1) The concentrations of the intracellular components, denoted e_i, x_i, and c^-, are based on the dry weight of the cells (g per g dry weight of cells, i.e. g gdw^{-1}). The concentrations of the exogenous substrate and cells, denoted s_i and c, are based on the volume of the reactor (g/L and gdw/L, respectively). The rates of all the processes are based on the dry weight of the cells (g gdw^{-1} h^{-1}). We shall use the term *specific rate* to emphasize this point.
The choice of these units implies that if the concentration of any intracellular component, Z, is z g gdw^{-1}, then the evolution of z in batch cultures is given by

$$\frac{dz}{dt} = r_z^+ - r_z^- - \left(\frac{1}{c}\frac{dc}{dt}\right)z,$$

where r_z^+ and r_z^- denote the specific rates of synthesis and degradation of Z in g gdw^{-1} h^{-1}.
(2) The transport and peripheral catabolism of S_i is catalysed by the "lumped" system of peripheral enzymes, E_i. The specific uptake rate of S_i, denoted

$r_{s,i}$, follows the modified Michaelis–Menten kinetics, $r_{s,i} \equiv V_{s,i}e_i s_i/(K_{s,i} + s_i)$.
(3) Part of the internalized substrate, denoted X_i, is converted to C^-. The remainder is oxidized to CO_2 in order to generate energy.
  (a) The conversion of X_i to C^- and CO_2 follows first-order kinetics, i.e. $r_{x,i} \equiv k_{x,i}x_i$.
  (b) The fraction of X_i converted to C^- is a constant (parameter), denoted Y_i. Thus, the specific rate of synthesis of C^- from X_i is $Y_i r_{x,i}$.[5]
(4) The internalized substrate also induces the synthesis of E_i.
  (a) The specific synthesis rate of E_i follows Hill kinetics, i.e. $r_{e,i} \equiv V_{e,i}x_i^{n_i}/(K_{e,i}^{n_i} + x_i^{n_i})$, where $n_i = 1$ or 2. Kinetic analysis of the data shows that enzyme induction can be hyperbolic ($n_i = 1$) or sigmoidal ($n_i = 2$) (Yagil and Yagil, 1971).
  By appealing to a molecular model of induction, we can express n_i, $V_{e,i}$, and $K_{e,i}$ in terms of the parameters associated with repressor–operator and repressor–inducer binding. It is shown in Appendix A that the Yagil and Yagil model of induction implies that n_i is the number of inducer molecules that bind to 1 repressor molecule. Furthermore, if the enzyme is *inducible*,

$$V_{e,i} = v_{e,i}o_{t,i}, \quad K_{e,i}^{n_i} = \frac{K_{x,i}}{K_{o,i}}r_{t,i}, \tag{1}$$

  where $v_{e,i}$ is the enzyme synthesis rate per unit mass of operator; $o_{t,i}, r_{t,i}$ are the total concentrations of the operator and repressor (g gdw^{-1}), respectively; and $K_{x,i}, K_{o,i}$ are the dissociation constants for repressor–inducer and repressor–operator binding, respectively.
  (b) The synthesis of the enzymes occurs at the expense of the biosynthetic constituents, C^-.
  (c) Enzyme degradation is negligibly small.

Given these assumptions, the mass balances yield the equations

$$\frac{ds_i}{dt} = -r_{s,i}c, \; r_{s,i} \equiv V_{s,i}e_i\frac{s_i}{K_{s,i} + s_i}, \tag{2}$$

$$\frac{dx_i}{dt} = r_{s,i} - r_{x,i} - \left(\frac{1}{c}\frac{dc}{dt}\right)x_i, r_{x,i} \equiv k_{x,i}x_i, \tag{3}$$

$$\frac{de_i}{dt} = r_{e,i} - \left(\frac{1}{c}\frac{dc}{dt}\right)e_i, \quad r_{e,i} \equiv V_{e,i}\frac{x^{n_i}}{K_{e,i}^{n_i} + x^{n_i}}, \tag{4}$$

$$\frac{dc^-}{dt} = (Y_1 r_{x,1} + Y_2 r_{x,2}) - (r_{e,1} + r_{e,2}) - \left(\frac{1}{c}\frac{dc}{dt}\right)c^-. \tag{5}$$

Fig. 4. Kinetic scheme of the minimal model (Narang, 1998a).

[5]The so-called *conservative* substrates, such as nitrogen and phosphorus sources, are completely assimilated (as opposed to carbon sources, which are partially oxidized to generate energy). During growth on mixtures of such substrates, $Y_i = 1$ for both the substrates.
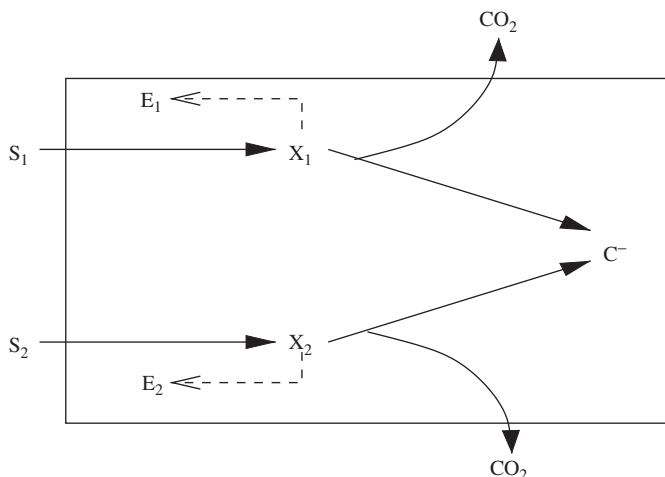
It is shown in Appendix B that since $x_1 + x_2 + e_1 + e_2 + c^- = 1$, Eqs. (3)–(5) implicitly define the specific growth rate, denoted r_g, and the evolution of the cell density via the relations

$$\frac{dc}{dt} = r_g c, \quad r_g \equiv \sum_{i=1}^{2} r_{s,i} - \sum_{i=1}^{2}(1 - Y_i)r_{x,i}. \tag{6}$$

Furthermore, since x_i is small, it attains quasisteady state on a time scale of seconds, thus resulting in the simplified equations

$$\frac{ds_i}{dt} = -r_{s,i}c, \tag{7}$$

$$x_i \approx \frac{V_{s,i}e_i s_i/(K_{s,i} + s_i)}{k_{x,i}}, \tag{8}$$

$$\frac{de_i}{dt} = r_{e,i} - r_g e_i, \quad r_{e,i} \approx V_{e,i}\frac{[e_i s_i/(K_{s,i} + s_i)]^{n_i}}{\bar{K}_{e,i}^{n_i} + [e_i s_i/(K_{s,i} + s_i)]^{n_i}},$$
$$\bar{K}_{e,i} \equiv K_{e,i}\frac{k_{x,i}}{V_{s,i}}, \tag{9}$$

$$\frac{dc}{dt} = r_g c, \quad r_g \approx Y_1 r_{s,1} + Y_2 r_{s,2}, \tag{10}$$

$$c^- = 1 - x_1 - x_2 - e_1 - e_2, \tag{11}$$

where (8) is obtained from the quasisteady state relation, i.e. $0 \approx r_{s,i} - r_{x,i}$.

We are particularly interested in the dynamics of the peripheral enzymes during the first exponential growth phase, since it is these finite-time dynamics that determine the substrate utilization pattern. If the peripheral enzymes for one of the substrates vanish during this period, there is diauxic growth; if the peripheral enzymes for both substrates persist, there is simultaneous substrate utilization.

It turns out that the motion of the enzymes during the first exponential growth phase is governed by only two equations. To see this, observe that during the first exponential growth phase, both substrates are in excess, i.e. $s_i \gg K_{s,i}$. Hence, even though the exogenous substrate concentrations are decreasing, the transport enzymes see a quasiconstant environment ($s_i/(K_{s,i} + s_i) \approx 1$), and approach the quasisteady state levels corresponding to exponential (balanced) growth. This motion is approximated by the equations

$$\frac{de_1}{dt} = V_{e,1}\frac{e_1^{n_1}}{\bar{K}_{e,1}^{n_1} + e_1^{n_1}} - (Y_1 V_{s,1}e_1 + Y_2 V_{s,2}e_2)e_1, \tag{12}$$

$$\frac{de_2}{dt} = V_{e,2}\frac{e_2^{n_2}}{\bar{K}_{e,2}^{n_2} + e_2^{n_2}} - (Y_1 V_{s,1}e_1 + Y_2 V_{s,2}e_2)e_2, \tag{13}$$

obtained from (9) by replacing $s_i/(K_{s,i} + s_i)$ with 1. We shall refer to these as the *reduced* equations. It should be emphasized that the steady states of the reduced equations are *quasisteady states* of the full system of equations (see

Narang et al., 1997a for a rigorous derivation of the reduced equations).

The reduced equations are formally similar to the equations of the standard Lotka–Volterra model for two competing species, namely,

$$\frac{dN_1}{dt} = r_1 N_1(1 - a_{11}N_1 - a_{12}N_2), \tag{14}$$

$$\frac{dN_2}{dt} = r_2 N_2(1 - a_{21}N_1 - a_{22}N_2), \tag{15}$$

where N_i is the population density of the ith species, r_i is the (unrestricted) specific growth rate of the ith species in the absence of any competition, and a_{i1}, a_{i2} are parameters that quantify the reduction of the unrestricted specific growth rate due to intra- and inter-specific competition (Murray, 1989). Thus, enzyme induction is the correlate of unrestricted growth, and the two dilution terms are the correlates of intra- and inter-specific competition. In what follows, we shall constantly appeal to this dynamical analogy.

The dynamics of the standard Lotka–Volterra model are well understood. Indeed, the bifurcation diagram of the model is completely determined by the two dimensionless parameters, $b_{21} \equiv a_{21}/a_{11}$ and $b_{12} \equiv a_{12}/a_{22}$ (Fig. 5). These parameters characterize the extent to which each species inhibits the other species relative to the extent to which it inhibits itself. Both species coexist precisely when they inhibit themselves more than they inhibit the other species, i.e. $b_{21}, b_{12} < 1$. Under all other conditions, coexistence is impossible. If the interaction between the species is
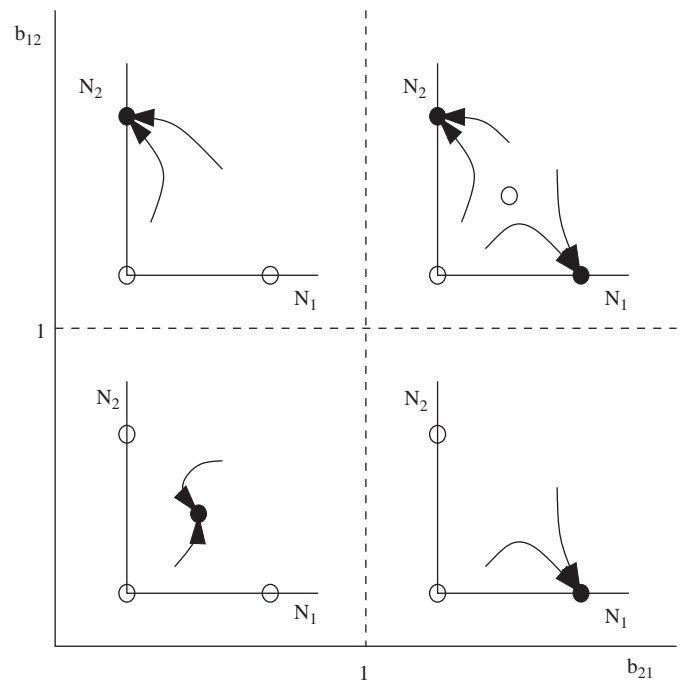

Fig. 5. Classification of the global dynamics for the standard Lotka–Volterra model. The full and open circles show stable and unstable steady states, respectively.

asymmetric ($b_{21} < 1, b_{12} > 1$ or $b_{21} > 1, b_{12} < 1$), one of them is rendered extinct (species 1 and 2, respectively). If both species inhibit the other species more than they inhibit themselves, i.e. $b_{21}, b_{12} > 1$, the outcome depends on the initial population densities.

Given the formal similarity of the reduced equations to the Lotka–Volterra model, we expect them to display "extinction" and "coexistence" dynamics. Importantly, these dynamics have simple biological interpretations. Extinction of one of the enzymes corresponds to diauxic growth, and coexistence of both enzymes corresponds to simultaneous consumption. It is therefore clear that the bifurcation diagram for the reduced equations is a useful analytical tool. It furnishes a classification of the substrate consumption patterns, which can then be used to systematically address the questions posed in the Introduction. Our first goal is to construct this bifurcation diagram.

To minimize the number of parameters in the bifurcation diagram, we rescale the reduced equations by defining the dimensionless variables

$$\varepsilon_i \equiv \frac{e_i}{\sqrt{V_{e,i}/(Y_i V_{s,i})}}, \quad \tau \equiv t\sqrt{V_{e,1} Y_1 V_{s,1}}.$$

The choice of the reference variables in this scaling is suggested by the following fact: $\sqrt{V_{e,i}/(Y_i V_{s,i})}$ and $\sqrt{V_{e,i} Y_i V_{s,i}}$ are upper bounds for the enzyme level and maximum specific growth rate attained during single-substrate exponential growth on saturating concentrations of S_i. Indeed, under these conditions, the mass balance for E_i becomes

$$0 = V_{e,i} \frac{e_i^{n_i}}{\bar{K}_{e,i}^{n_i} + e_i^{n_i}} - Y_i V_{s,i} e_i^2.$$

Hence, $e_i < \sqrt{V_{e,i}/(Y_i V_{s,i})}$, and the maximum specific growth rate on S_i, denoted $r_{g,i}^{\max}$, satisfies the relation

$$r_{g,i}^{\max} \approx Y_i V_{s,i} e_i < Y_i V_{s,i} \sqrt{\frac{V_{e,i}}{Y_i V_{s,i}}} = \sqrt{Y_i V_{s,i} V_{e,i}}.$$

The above scaling yields the dimensionless reduced equations

$$\frac{d\varepsilon_1}{d\tau} = \frac{\varepsilon_1^{n_1}}{\kappa_1^{n_1} + \varepsilon_1^{n_1}} - (\varepsilon_1 + \alpha\varepsilon_2)\varepsilon_1, \tag{16}$$

$$\frac{d\varepsilon_2}{d\tau} = \alpha \frac{\varepsilon_2^{n_2}}{\kappa_2^{n_2} + \varepsilon_2^{n_2}} - (\varepsilon_1 + \alpha\varepsilon_2)\varepsilon_2, \tag{17}$$

with dimensionless parameters

$$\kappa_i \equiv \frac{\bar{K}_{e,i}}{\sqrt{V_{e,i}/(Y_i V_{s,i})}} = K_{e,i} k_{x,i} \sqrt{\frac{Y_i}{V_{s,i} V_{e,i}}}$$

$$= k_{x,i} \left(\frac{K_{x,i} r_{t,i}}{K_{o,i}}\right)^{1/n_i} \sqrt{\frac{Y_i}{V_{s,i} V_{e,i}}}, \tag{18}$$

$$\alpha \equiv \frac{\sqrt{V_{e,2} Y_2 V_{s,2}}}{\sqrt{V_{e,1} Y_1 V_{s,1}}}. \tag{19}$$

These dimensionless parameters have simple biological interpretations. We can view κ_i as a dimensionless saturation constant for induction, and α as a measure of the maximum specific growth rate on S_2 relative to that on S_1.

3. Results

We wish to construct the bifurcation diagram for Eqs. (16)–(17). Since limit cycles are impossible in Lotka–Volterra models for competing species (Hirsch and Smale, 1974), it suffices to determine the steady states and their stability.

Eqs. (16)–(17) admit at most four types of steady states: the trivial steady state ($\varepsilon_1 = \varepsilon_2 = 0$), the semitrivial steady states ($\varepsilon_1 > 0, \varepsilon_2 = 0$ and $\varepsilon_1 = 0, \varepsilon_2 > 0$), and the non-trivial steady state, $\varepsilon_1, \varepsilon_2 > 0$. We denote these steady states by E_{00}, E_{10}, E_{01}, and E_{11}, respectively.

We shall consider two cases: $n_1 = n_2 = 1$ and $n_1 = 2$, $n_2 = 1$. The second case will serve to show the qualitative changes engendered by sigmoidal induction kinetics.

3.1. Case 1 ($n_1 = n_2 = 1$)

In this case, the scaled equations are

$$\frac{d\varepsilon_1}{dt} = \frac{\varepsilon_1}{\kappa_1 + \varepsilon_1} - (\varepsilon_1 + \alpha\varepsilon_2)\varepsilon_1,$$

$$\frac{d\varepsilon_2}{dt} = \alpha \frac{\varepsilon_2}{\kappa_2 + \varepsilon_2} - (\varepsilon_1 + \alpha\varepsilon_2)\varepsilon_2.$$

The bifurcation diagrams for these equations are shown in Fig. 6. They were inferred from the following facts derived in Appendix C:

(1) The trivial steady, E_{00}, always exists (for all $\alpha, \kappa_1, \kappa_2 > 0$), but it is always unstable (as a node).
(2) The semitrivial steady state, E_{10}, always exists. It is (uniquely) given by

$$\varepsilon_1 = \frac{-\kappa_1 + \sqrt{\kappa_1^2 + 4}}{2}, \quad \varepsilon_2 = 0,$$

and is stable (as a node) precisely if $\varepsilon_1|_{E_{10}}$ exceeds α/κ_2, the ε_1-intercept of the non-trivial nullcline for ε_2.[6] i.e.

$$\varepsilon_1|_{E_{10}} > \frac{\alpha}{\kappa_2} \Leftrightarrow \alpha < \alpha_*(\kappa_1, \kappa_2) \equiv \frac{\kappa_2(-\kappa_1 + \sqrt{\kappa_1^2 + 4})}{2}. \tag{20}$$

---

[6] The nullclines for ε_i refer to the locus of points on the $\varepsilon_1\varepsilon_2$-plane at which $d\varepsilon_i/dt = 0$. In the case of the reduced equations, the nullclines for ε_i consist of two curves. One of these curves is the *trivial* nullcline, $\varepsilon_i = 0$; the other curve is called the *non-trivial* nullcline.
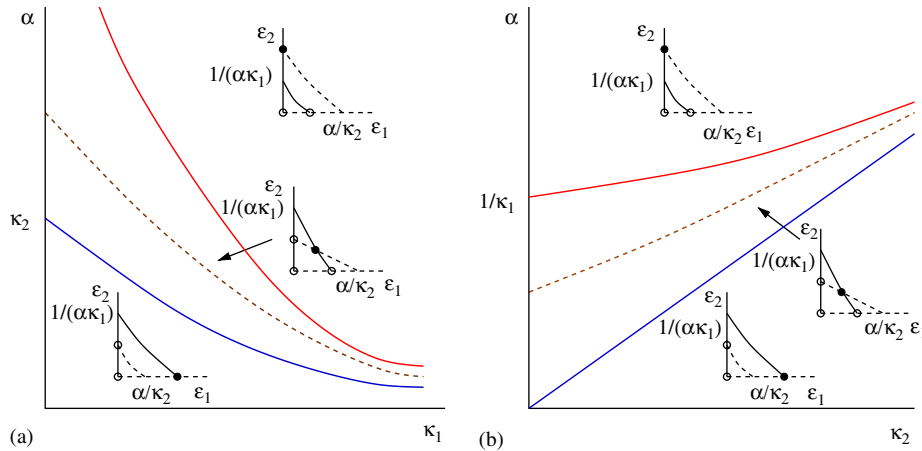
Fig. 6. Bifurcation diagrams for the case $n_1 = n_2 = 1$ at (a) fixed $\kappa_2 > 0$ and (b) fixed $\kappa_1 > 0$. In the phase portraits, the nullclines for ε_1 and ε_2 are represented by full and dashed lines, respectively; stable and unstable steady states are represented by full and open circles, respectively. The graphs of α_*, α^*, and α_g are represented by blue, red, and dashed brown curves.

(3) The steady state, E_{01}, always exists. It is given by

$$\varepsilon_1 = 0, \quad \varepsilon_2 = \frac{-\kappa_2 + \sqrt{\kappa_2^2 + 4}}{2},$$

and it is stable (as a node) precisely if $\varepsilon_2|_{E_{01}}$ exceeds $1/(\alpha\kappa_1)$, the ε_2-intercept of the non-trivial nullcline for ε_1, i.e.

$$\varepsilon_2|_{E_{01}} > \frac{1}{\alpha\kappa_1} \Leftrightarrow \alpha > \alpha^*(\kappa_1, \kappa_2) \equiv \frac{2}{\kappa_1\left(-\kappa_2 + \sqrt{\kappa_2^2 + 4}\right)}. \tag{21}$$

(4) The surface of $\alpha_*(\kappa_1, \kappa_2)$ lies below the surface of $\alpha^*(\kappa_1, \kappa_2)$, i.e.

$$\alpha_*(\kappa_1, \kappa_2) < \alpha^*(\kappa_1, \kappa_2) \tag{22}$$

for all $\kappa_1, \kappa_2 > 0$. The notation was chosen to reflect this fact: The functions, $\alpha_*(\kappa_1, \kappa_2)$ and $\alpha^*(\kappa_1, \kappa_2)$, represent the lower and upper surfaces of the bifurcation diagram.

(5) The steady state, E_{11}, exists if and only if both E_{10} and E_{01} are unstable, i.e.

$$\alpha_*(\kappa_1, \kappa_2) < \alpha < \alpha^*(\kappa_1, \kappa_2). \tag{23}$$

It is unique and stable whenever it exists.

The bifurcation diagrams imply the following classification of the substrate utilization patterns:

(1) If $\alpha < \alpha_*(\kappa_1, \kappa_2)$, only E_{10} is stable, which corresponds to preferential consumption of S_1.
(2) If $\alpha_*(\kappa_1, \kappa_2) < \alpha < \alpha^*(\kappa_1, \kappa_2)$, only E_{11} is stable, and there is simultaneous consumption of S_1 and S_2.
(3) If $\alpha > \alpha^*(\kappa_1, \kappa_2)$, only E_{01} is stable, which corresponds to preferential consumption of S_2.

Thus, the surfaces of $\alpha_*(\kappa_1, \kappa_2)$ and $\alpha^*(\kappa_1, \kappa_2)$ delineate the boundaries of the substrate consumption patterns.[7]

If the point, $(\kappa_1, \kappa_2, \alpha)$, crosses either one of these boundaries, there is an abrupt transition in the substrate consumption pattern due to a transcritical bifurcation. This becomes evident if α is increased at any fixed $\kappa_1, \kappa_2 > 0$ (Fig. 7). At $\alpha = \alpha_*(\kappa_1, \kappa_2)$, the substrate consumption pattern switches from preferential consumption of S_1 to simultaneous consumption of S_1 and S_2 through a transcritical bifurcation in which E_{10} (red curve) yields its stability to E_{11} (black curve). As α is increased further, there is another transition at $\alpha = \alpha^*(\kappa_1, \kappa_2)$ wherein simultaneous consumption switches to preferential consumption of S_2 via a transcritical bifurcation involving the transfer of stability from E_{11} (black curve) to E_{01} (blue curve).

We gain intuitive insight into the bifurcation diagram by considering two limiting cases. Fig. 6 shows that if κ_1 or κ_2 are large, the curves for α_* and α^* converge, and simultaneous consumption is virtually impossible. In contrast, if both κ_1 and κ_2 are small, there is simultaneous consumption for almost all α. To understand these limiting cases, observe that when κ_1, κ_2 are large, Eqs. (16)–(17) are approximated by the equations

$$\frac{d\varepsilon_1}{dt} \approx \frac{1}{\kappa_1}\varepsilon_1(1 - \kappa_1\varepsilon_1 - \alpha\kappa_1\varepsilon_2)\varepsilon_1,$$

$$\frac{d\varepsilon_2}{dt} \approx \frac{\alpha}{\kappa_2}\varepsilon_2\left(1 - \frac{\kappa_2}{\alpha}\varepsilon_1 - \kappa_2\varepsilon_2\right)\varepsilon_2,$$

which are formally identical to the standard Lotka–Volterra model with $a_{11} = \kappa_1$, $a_{12} = \alpha\kappa_1$, $a_{21} = \kappa_2/\alpha$, and $a_{22} = \kappa_2$. However, there is an important difference. The parameters, $b_{21} \equiv a_{21}/a_{11}$, $b_{12} \equiv a_{12}/a_{22}$, are not indepen-

---

[7] An analogous classification is also obtained when the model is extended to continuous cultures (Narang, 1998b, Fig. 10). However, the control parameters consist of the dilution rate and feed concentrations (rather than the physiological parameters, α, κ_1, and κ_2).
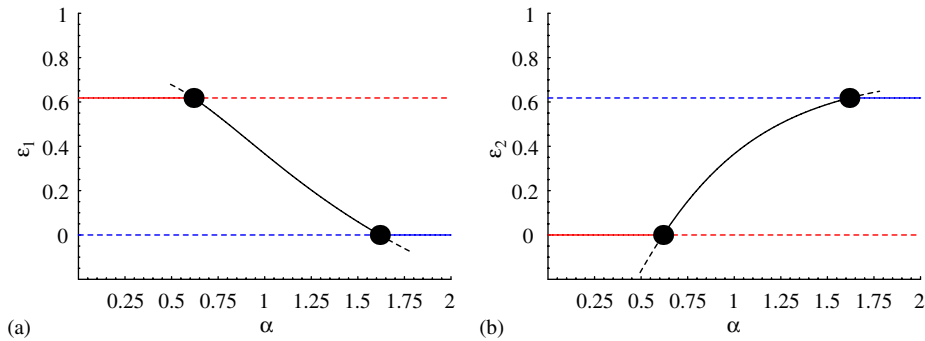
Fig. 7. The bifurcation diagram obtained when α is increased at $\kappa_1 = \kappa_2 = 1$. The red, blue, and black curves represent the locus of E_{10}, E_{01}, and E_{11}, respectively. The curves are full (resp., dashed) if the steady state is stable (resp., unstable). The bifurcation points at $\alpha = \alpha_*(1,1) = 0.62$ and $\alpha = \alpha^*(1,1) = 1.62$ are represented by full circles.

dent since $b_{21} = \kappa_2/(\alpha\kappa_1) = 1/b_{12}$. But if b_{12} and b_{21} are restricted to the curve $b_{21}b_{12} = 1$, Fig. 5 implies that coexistence (i.e. simultaneous consumption) is impossible: E_1 becomes extinct if $b_{21} < 1$, and E_2 becomes extinct if $b_{21} > 1$. On the other hand, if κ_1, κ_2 are small, the enzyme synthesis rate is essentially constant (quasiconstitutive). The enzymes therefore resist extinction, and coexist for almost all α.

3.1.1. Dependence of substrate consumption pattern on genotype

In the experimental literature, the influence of the physiological parameters is often studied by altering the genetic make-up (genotype) of the cells, and observing the resultant change in the substrate consumption pattern (phenotype) of the cells. We show below that the bifurcation diagrams are consistent with the phenotypic changes observed in response to various genotypic alterations.

Before doing so, however, it is useful to note that in all the experiments described below, the phenotype of the wild-type strain is preferential consumption of a substrate (glucose, in most cases). Since Eqs. (16) and (17) are formally the same, there is no loss of generality in assuming that the preferred substrate is S_2, and the parameters, $\kappa_1, \kappa_2, \alpha$, for the wild-type strain lie in the region, $\alpha > \alpha^*$ (above the red curve in Fig. 6).

We begin by considering the cases in which the genetic perturbation transforms the substrate consumption pattern from preferential to simultaneous consumption.

In wild-type E. coli, transcription of lac is abolished in the presence of glucose. However, mutants with lesions in the lac operator synthesize β-galactosidase even in the presence of glucose (Jacob and Monod, 1961). Thus, the mutation transforms the substrate consumption pattern from preferential consumption of glucose to simultaneous consumption of glucose and lactose. The very same phenotypic change is also observed in mutants with a defective lacI, the gene encoding the lac repressor (Jacob and Monod, 1961). To explain these phenotypic changes in terms of the model, observe that mutations in the lac operator or lacI impair the lac repressor–operator binding,

i.e. they increase the dissociation constant, $K_{o,1}$. It follows from Eqs. (18)–(19) that κ_1 decreases at fixed κ_2 and α. Inspection of Fig. 6a shows that such a change can shift the substrate consumption pattern from preferential consumption of S_2 to simultaneous consumption.

If lacY, the gene encoding lactose permease, is overexpressed in E. coli PR166, synthesis of β-galactosidase persists in the presence of glucose (Fig. 8a). Now, in the model, overexpression of lacY corresponds to higher $V_{e,1}$. It follows from Eqs. (18)–(19) that κ_1, α decrease at fixed κ_2, and Fig. 6a implies that the observed phenotype is indeed feasible.

In E. coli PR166, β-galactosidase is synthesized despite the presence of glucose if crr, the gene for enzyme IIA^{glc}, is deleted (Fig. 8a). Similarly, in the wild-type strain, E. coli K12 W3110, glucose is consumed before galactose. However, mutants with lesions in a gene encoding a transport enzyme for glucose consume the two substrates simultaneously (Kamogawa and Kurahashi, 1967). In these cases, the effect of the mutation is to decrease $V_{s,2}$, so that κ_2 increases and α decreases at fixed κ_1. It follows from Fig. 6b that such a change could lead to simultaneous consumption of the substrates.

Now, all the mutant phenotypes discussed above can be explained just as well by alternative hypotheses appealing only to the molecular mechanisms. Indeed, the first case is obviously due to impaired repressor–operator binding, and one can argue that the remaining two cases are due to diminished inducer exclusion. However, the next two examples, which involve the reversal of the diauxie, are difficult to explain from the molecular point of view.

Fig. 9a shows that in E. coli Hfr3000, glucose is consumed before galactose. However, the mutant strain MM6, which contains a lesion in the PTS enzyme I (Tanaka et al., 1967), consumes galactose before glucose (Fig. 9b). Likewise, E. coli strain 159 consumes mannitol before sorbitol (Fig. 9c), but the corresponding mutant strain 157, which contains a lesion in the PTS enzyme II^{mtl}, consumes sorbitol before mannitol (Fig. 9d). These phenotypic changes fall within the scope of the minimal model. In both mutants, the transport enzyme for the
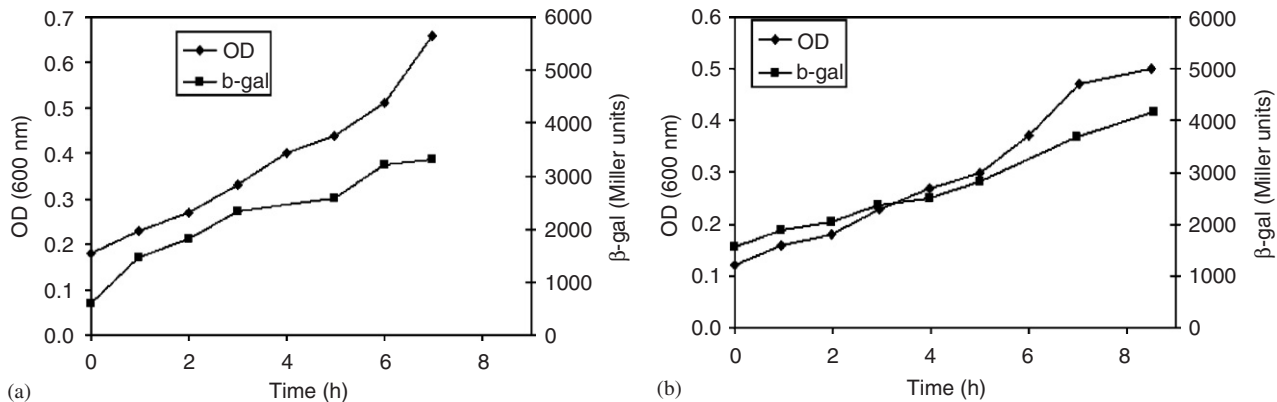
Fig. 8. In *E. coli* PR166, synthesis of *β*-galactosidase persists in the presence of glucose if (a) *lac Y* is overexpressed or (b) *crr*, the gene for enzyme IIA^{glc}, is deleted (Kimata et al., 1997). The mutant cells in (b) grow on glucose despite the absence of IIA^{glc} because of slow uptake of glucose by the PTS enzymes for mannose.
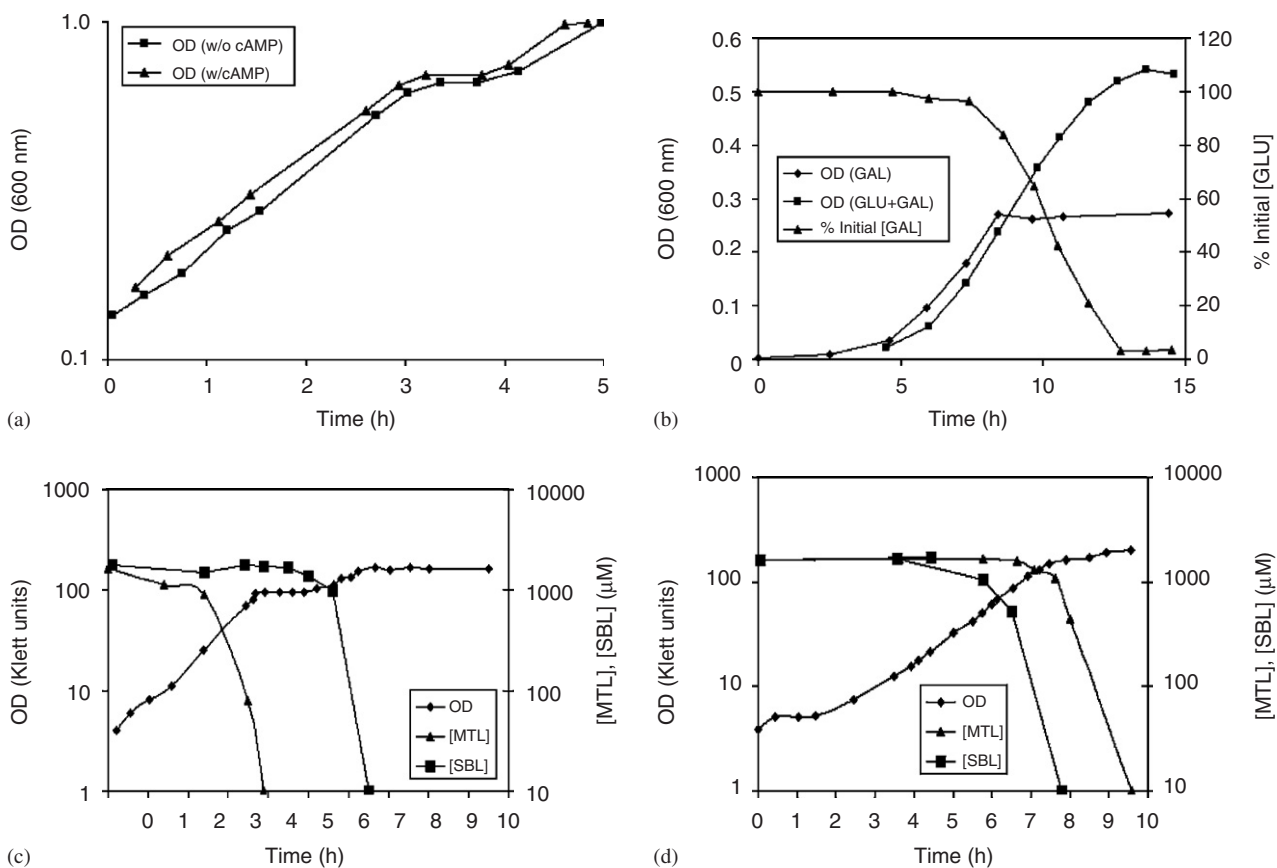

Fig. 9. Reversal of the diauxie in mutants of *E. coli*: *Upper panel*: (a) in strain Hfr3000, glucose is consumed before galactose (Joseph et al., 1981). The optical density (OD) shows a pronounced diauxic lag, regardless of the presence of cAMP in the culture. (b) In the corresponding PTS-deficient strain, galactose is consumed before glucose (Asensio et al., 1963). Note that the evolution of the OD during the first 8 h is the same during growth on galactose (OD (GAL)) and glucose + galactose (OD (GLU + GAL)). Furthermore, there is no consumption of glucose during this period. *Lower panel:* (c) In strain 159, mannitol (MTL) is consumed before sorbitol (SBL). (d) In the corresponding enzyme II^{mtl}-deficient strain, sorbitol is consumed before mannitol (Lengeler and Lin, 1972).

preferred substrate is impaired, i.e. $V_{s,2}$ decreases, so that κ_1 remains unchanged, but κ_2 increases and α decreases. If the changes in κ_2 and α are sufficiently large, Fig. 6b implies that the substrate consumption pattern will shift

from preferential consumption of S_2 to preferential consumption of S_1.

It should be emphasized that the "reversal of the diauxie" is a natural consequence of the minimal model.

This is because each enzyme inhibits the other enzyme due to dilution by growth, i.e. the inhibition is *mutual* or *competitive*. Consequently, suppressing the uptake (and hence, the growth) on one of the substrates automatically tilts the balance of power in favor of the other substrate. In contrast, the "reversal of the diauxie" is difficult to explain in terms of molecular mechanisms alone. This is because in all the molecular mechanisms, the inhibition is *unilateral* rather than mutual. In *E. coli*, for instance, there are numerous mechanisms that allow PTS sugars, such as glucose and mannitol, to inhibit the synthesis of the enzymes for non-PTS substrates. But there is no mechanism for non-PTS substrates to inhibit the synthesis of PTS enzymes. This difficulty did not escape the attention of Asensio et al., who observed the reversal of the glucose–galactose diauxie (Fig. 9, top panel). Faced with the "reversal of the diauxie," they were compelled to conclude that the "diauxie is, at least in part, due to competitive effects at the permease level."

3.1.2. Dependence of substrate consumption pattern on relative growth rates

In order to consider the relationship between the substrate consumption pattern and the ratio of the single-substrate maximum specific growth rates, define

$$\rho \equiv \frac{r_{g,2}^{\max}}{r_{g,1}^{\max}},$$

where $r_{g,i}^{\max}$ denotes maximum specific growth rate during single-substrate growth on saturating concentrations of S_i. Now, the model implies that

$$r_{g,1}^{\max} = Y_1 V_{s,1} e_1|_{E_{10}} = \sqrt{V_{e,1} Y_1 V_{s,1}} \varepsilon_1|_{E_{10}},$$

$$r_{g,2}^{\max} = Y_2 V_{s,2} e_2|_{E_{01}} = \sqrt{V_{e,2} Y_2 V_{s,2}} \varepsilon_2|_{E_{01}},$$

so that

$$\rho = \alpha \frac{\varepsilon_2|_{E_{01}}}{\varepsilon_1|_{E_{10}}} = \frac{\alpha}{\alpha_g(\kappa_1, \kappa_2)},$$

$$\alpha_g(\kappa_1, \kappa_2) \equiv \frac{\varepsilon_1|_{E_{10}}}{\varepsilon_2|_{E_{01}}} = \frac{-\kappa_1 + \sqrt{\kappa_1^2 + 4}}{-\kappa_2 + \sqrt{\kappa_2^2 + 4}}.$$

It follows that

(1) The surface of $\alpha_g(\kappa_1, \kappa_2)$ separates the parameter space into two distinct regions: above the surface, $\rho > 1$, i.e. $r_{g,2}^{\max} > r_{g,1}^{\max}$, and below the surface, $\rho < 1$, i.e. $r_{g,2}^{\max} < r_{g,1}^{\max}$.
(2) The surface of $\alpha_g(\kappa_1, \kappa_2)$ lies between the surfaces of $\alpha_*(\kappa_1, \kappa_2)$ and $\alpha^*(\kappa_1, \kappa_2)$, i.e.

$$\alpha_*(\kappa_1, \kappa_2) < \alpha_g(\kappa_1, \kappa_2) < \alpha^*(\kappa_1, \kappa_2) \quad (24)$$

for all $\kappa_1, \kappa_2 > 0$ (see Appendix C). Thus, the graph of α_g, denoted by the dashed brown line in Fig. 6, lies between the graphs of α_* (blue curve) and α^* (red curve).

Given these results, we can recast the classification of the substrate consumption patterns in terms of ρ.

To this end, define

$$\rho_*(\kappa_2) \equiv \frac{\alpha_*(\kappa_1, \kappa_2)}{\alpha_g(\kappa_1, \kappa_2)} = \kappa_2 \frac{-\kappa_2 + \sqrt{\kappa_2^2 + 4}}{2},$$

$$\rho^*(\kappa_1) \equiv \frac{\alpha^*(\kappa_1, \kappa_2)}{\alpha_g(\kappa_1, \kappa_2)} = \frac{1}{\kappa_1} \frac{2}{-\kappa_1 + \sqrt{\kappa_1^2 + 4}}.$$

Then, there is preferential consumption of S_1 (resp., S_2) precisely when $\rho < \rho_*(\kappa_2)$ (resp., $\rho > \rho^*(\kappa_1)$), and simultaneous consumption if and only if $\rho_*(\kappa_2) < \rho < \rho^*(\kappa_1)$. Thus, ρ_* and ρ^* define the limits of ρ at which there is simultaneous consumption. It turns out that $\rho_*(\kappa_2)$ increases from 0 to 1 as κ_2 goes from 0 to ∞, and $\rho^*(\kappa_1)$ decreases from ∞ to 0 as κ_1 goes from 0 to ∞ (Fig. 10). We are now ready to discuss the relationship between the substrate consumption patterns and the ratio of the single-substrate maximum specific growth rates.

The Harder and Dijkhuizen correlation states that when growth is diauxic, the preferred substrate is the one that, by itself, supports a higher maximum specific growth rate (p. 9). The model predictions are consistent with this correlation. This is already evident from Fig. 6: $\alpha < \alpha_g$, i.e. $\rho < 1$ in the region, $\alpha < \alpha_*$, corresponding to preferential consumption of S_1, and $\alpha > \alpha_g$, i.e. $\rho > 1$ in the region $\alpha > \alpha^*$ corresponding to preferential consumption of S_2. The same property is also manifested in Fig. 10, e.g. in the region, $\rho < \rho_*(\kappa_2)$, corresponding to preferential consumption of S_1, $\rho < 1$ because the graph of $\rho_*(\kappa_2)$ is always below 1. The manifestation of the Harder–Dijkhuizen correlation in this minimal model suggests that is an intrinsic property of the induction and dilution kinetics. It can be explained without invoking goal-oriented regulatory mechanisms, which form the basis of models based on optimality principles (Kompala et al., 1986; Mahadevan et al., 2002; Ramakrishna et al., 1996).

Current experimental evidence suggests that the existence of comparable single-substrate maximum specific
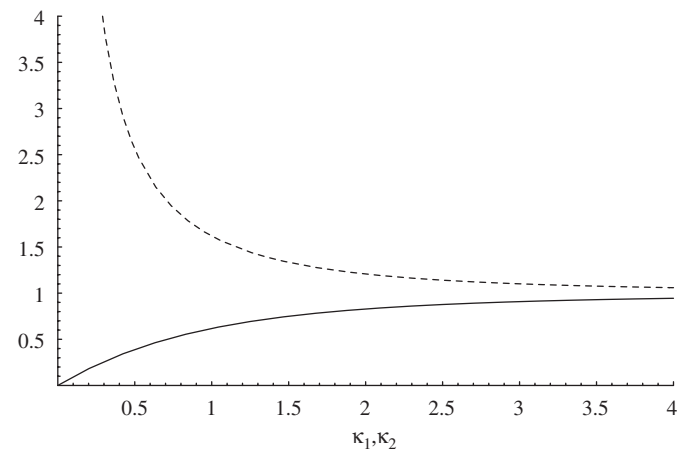
Fig. 10. Classification of substrate consumption patterns in terms of ρ, the ratio of the single-substrate maximum specific growth rates. The full and dashed lines show the graphs of $\rho_*(\kappa_2)$ and $\rho^*(\kappa_1)$, respectively.

growth rates is, perhaps, necessary but not sufficient for simultaneous consumption (p. 11). However, Fig. 10 shows that this condition ($\rho \approx 1$) is neither necessary nor sufficient for simultaneous consumption. It is not necessary because when $\kappa_1, \kappa_2 \ll 1$, there is simultaneous consumption for almost all ρ. It is not sufficient for simultaneous consumption because when $\kappa_1, \kappa_2 \gg 1$, simultaneous consumption is virtually impossible—it cannot be obtained unless ρ lies in a vanishingly small neighborhood of 1. These results can be understood in terms of the limiting cases discussed above. If κ_1, κ_2 are small, the enzymes are quasiconstitutive, and they resist extinction, regardless of the maximum specific growth rates. As κ_1 and κ_2 increase, the enzymes become progressively more vulnerable to extinction, and in the limit of large κ_1, κ_2, they cannot coexist.

We note finally that unlike the standard Lotka–Volterra model for competing species, there are no parameter values that yield bistable enzyme dynamics (compare Figs. 5 and 6). We show below that bistability becomes feasible when the induction kinetics are sigmoidal.

3.2. Case 2 ($n_1 = 2$, $n_2 = 1$)

In this case, the scaled equations are

$$\frac{d\varepsilon_1}{dt} = \frac{\varepsilon_1^2}{\kappa_1^2 + \varepsilon_1^2} - (\varepsilon_1 + \alpha\varepsilon_2)\varepsilon_1,$$

$$\frac{d\varepsilon_2}{dt} = \alpha \frac{\varepsilon_2}{\kappa_2 + \varepsilon_2} - (\varepsilon_1 + \alpha\varepsilon_2)\varepsilon_2.$$

The key results, which are shown in detail in Appendix D, are as follows:

(1) The trivial steady, E_{00}, always exists, regardless of the parameter values. It is always unstable.
(2) The semitrivial steady state, E_{10}, exists if and only if $\kappa_1 < 1$, in which case it is unique, and given by

$$\varepsilon_1 = \sqrt{1 - \kappa_1^2}, \quad \varepsilon_2 = 0.$$

It is stable (as a node) if and only if $\varepsilon_1|_{E_{10}}$ exceeds the ε_1-intercept of the non-trivial nullcline for ε_2, i.e.

$$\varepsilon_1|_{E_{10}} > \frac{\alpha}{\kappa_2} \Leftrightarrow \alpha < \kappa_2\sqrt{1 - \kappa_1^2} \equiv \alpha_*(\kappa_1, \kappa_2). \quad (25)$$

(3) The semitrivial steady state, E_{01}, always exists, and is given by

$$\varepsilon_1 = 0, \quad \varepsilon_2 = \frac{-\kappa_2 + \sqrt{\kappa_2^2 + 4}}{2}. \quad (26)$$

It is always stable (as a node).
(4) Non-trivial steady states exist only if $\kappa_1 < 1$. Under these conditions, there are at most two non-trivial

steady states. There is a unique non-trivial steady state if and only if

$$0 < \alpha < \alpha_*(\kappa_1, \kappa_2),$$

and it is unstable whenever it exists. There are two non-trivial steady states if and only if

$$0 < \kappa_1 < \beta \equiv \sqrt{\frac{2 + \kappa_2^2}{2(1 + \kappa_2^2)}}, \quad \alpha_*(\kappa_1, \kappa_2) < \alpha < \alpha^*(\kappa_1, \kappa_2),$$

where $\alpha^*(\kappa_1, \kappa_2)$ is the value of α at which the non-trivial nullclines for ε_1 and ε_2 touch. One of these steady states is stable and the other is unstable.
(5) The surface of $\alpha_*(\kappa_1, \kappa_2)$ lies below the surface of $\alpha^*(\kappa_1, \kappa_2)$ for all $0 < \kappa_1 < \beta$ and $\kappa_2 > 0$.

The bifurcation diagram shown in Fig. 11 implies the following classification of the substrate utilization patterns.

(1) If $\alpha < \alpha_*$, E_{10} and E_{01} are stable, i.e. there is preferential consumption of S_1 or S_2, depending on the initial conditions.
(2) If $0 < \kappa_1 < \beta$ and $\alpha_* < \alpha < \alpha^*$, E_{01} and E_{11} are stable, i.e. there is preferential consumption of S_2 or simultaneous consumption of S_1 and S_2, depending on the initial conditions.
(3) If $\beta < \kappa_1 < 1, \alpha > \alpha_*$ or $\kappa_1 > 1$, there is preferential consumption of S_2, regardless of the initial conditions.
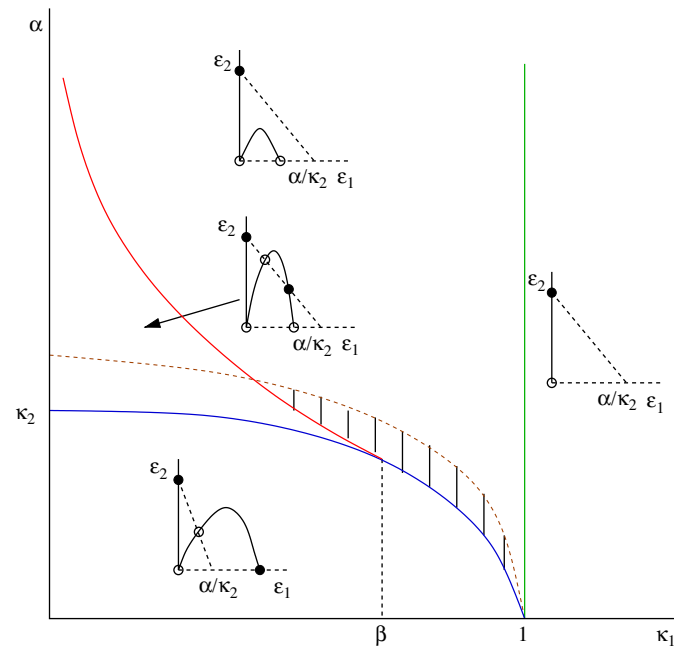

Fig. 11. The bifurcation diagram for the case $n_1 = 2$, $n_2 = 1$ at any fixed $\kappa_2 > 0$. In the phase portraits, the nullclines for ε_1 and ε_2 are represented by full and dashed lines, respectively; stable and unstable steady states are represented by full and open circles, respectively. The graphs of α_*, α^*, $\kappa_1 = 1$, and α_g are represented by blue, red, green, and dashed brown curves, respectively. In the hatched region, S_2 is the preferred substrate for all preculturing conditions, even though it supports a maximum specific growth rate lower than that on S_1.
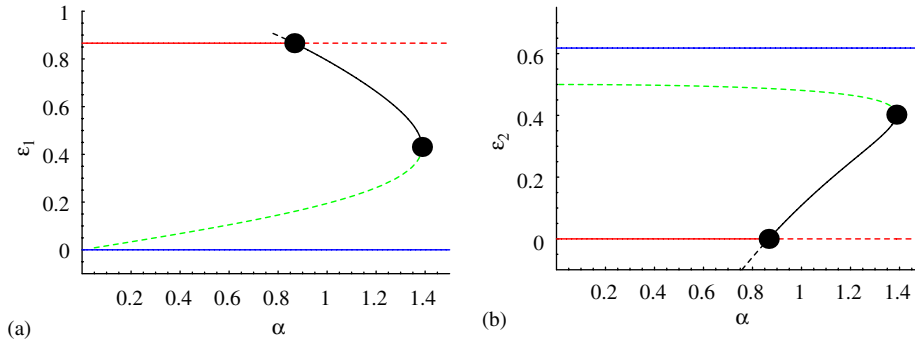
Fig. 12. The bifurcation diagram obtained when α is increased at $\kappa_1 = 0.5$ and $\kappa_2 = 1$. The red and blue curves show the semitrivial steady states, E_{10}, E_{01}, respectively. The green and black curves show the two non-trivial states (E_{11}). The curves are full (resp., dashed) if the corresponding steady state is stable (resp., full). The bifurcation points are represented by full circles.

The surfaces of α_* and α^* define the locus of transcritical and fold (saddle-node) bifurcations, respectively (Fig. 12). If α is increased at any fixed $0 < \kappa_1 < \beta$ and $\kappa_2 > 0$, the substrate consumption pattern changes at $\alpha = \alpha_*$ from bistable dynamics involving preferential consumption of S_1 or S_2 to bistable dynamics involving preferential consumption of S_2 or simultaneous consumption. This transition occurs via a transcritical bifurcation. At $\alpha = \alpha^*$, the substrate consumption pattern switches to preferential consumption of S_2 via a fold bifurcation.

Comparison of Fig. 11 with Fig. 6 shows that certain features are preserved. Specifically, preferential consumption of S_1 is feasible only at low α, and simultaneous consumption occurs only if α has intermediate values and κ_1, κ_2 are not too large. However, a unique property emerges in Fig. 11, namely, bistability. This is due to the sigmoidal induction kinetics for E_1, which ensure that preferential consumption of S_2 is feasible at all parameter values.

It is also worth examining the relationship between the classification predicted by the model and the empirical classification based on the single-substrate maximum specific growth rates. In this case

$$\rho = \alpha \frac{\varepsilon_2|_{E_{01}}}{\varepsilon_1|_{E_{10}}} = \frac{\alpha}{\alpha_g(\kappa_1, \kappa_2)}, \quad \alpha_g \equiv \frac{2\sqrt{1 - \kappa_1^2}}{-\kappa_2 + \sqrt{\kappa_2^2 + 4}}.$$

Now, $\alpha_g > \alpha_*$ because $-\kappa_2 + \sqrt{\kappa_2^2 + 4} < 2/\kappa_2$ (see Appendix C). Furthermore, α_g is zero at $\kappa_1 = 1$. Thus, the graph of α_g lies above the graph of α_* (dashed brown line in Fig. 11). This implies that a substrate can be consumed preferentially even if it supports a lower maximum specific growth rate. Indeed, if the parameters lie in the region, $\alpha < \alpha_g$, then S_2 supports a lower maximum specific growth rate than S_1, and yet, cells precultured on S_2 consume this substrate preferentially. If the parameter values lie in the hatched region of Fig. 11, S_2 is the preferred substrate, regardless of the manner in which the cells are precultured.

3.2.1. Evidence of bistable substrate consumption patterns

The bistable dynamics predicted by Fig. 11 have been observed in experiments.

The bistable dynamics in the region, $\alpha_* < \alpha < \alpha^*$, correspond to preferential consumption of S_2 if the preculture is grown on S_2, and simultaneous consumption if the preculture is grown on S_1. Two examples of this substrate consumption pattern were described in the Introduction, namely, growth of *P. aeruginosa* on glucose plus citrate (Hamilton and Dawes, 1959, 1960, 1961) and growth of *E. coli* K12 on a mixture of glucose and pyruvate (Narang et al., 1997b). Fig. 13 shows another example of this substrate consumption pattern. When *Streptococcus mutans* GS5 is grown on a mixture of glucose and lactose, glucose-precultured cells consume glucose before lactose (Fig. 13a), whereas lactose-precultured cells consume both glucose and lactose (Fig. 13b).

The bistable dynamics in the region, $\alpha < \alpha_*$, correspond to preferential consumption of S_1 if the preculture is grown on S_1, and preferential consumption of S_2 if the preculture is grown on S_2. Furthermore, the maximum specific growth on S_2 is lower than that on S_1. There is evidence suggesting the existence of this substrate consumption pattern. Tsuchiya and coworkers studied the growth of *Salmonella typhimurium* on a mixture of glucose and melibiose (Kuroda et al., 1992; Okada et al., 1981). They found that the wild-type strain LT2 consumed glucose before melibiose. However, the PTS enzyme I mutant, SB1476, yielded the bistable substrate consumption pattern corresponding to the region, $\alpha < \alpha_*$. Cells precultured on glucose consumed glucose preferentially (Fig. 13c), and cells precultured on melibiose consumed melibiose preferentially (Fig. 13d). Moreover, the maximum specific growth rate on glucose ($0.24\,h^{-1}$) is significantly lower than that on melibiose ($0.41\,h^{-1}$). It should be noted that these experiments were done in the presence of $5\,mM$ cAMP in the culture. However, at least in the case of glucose-precultured cells, the same phenotype was observed even in the absence of cAMP.
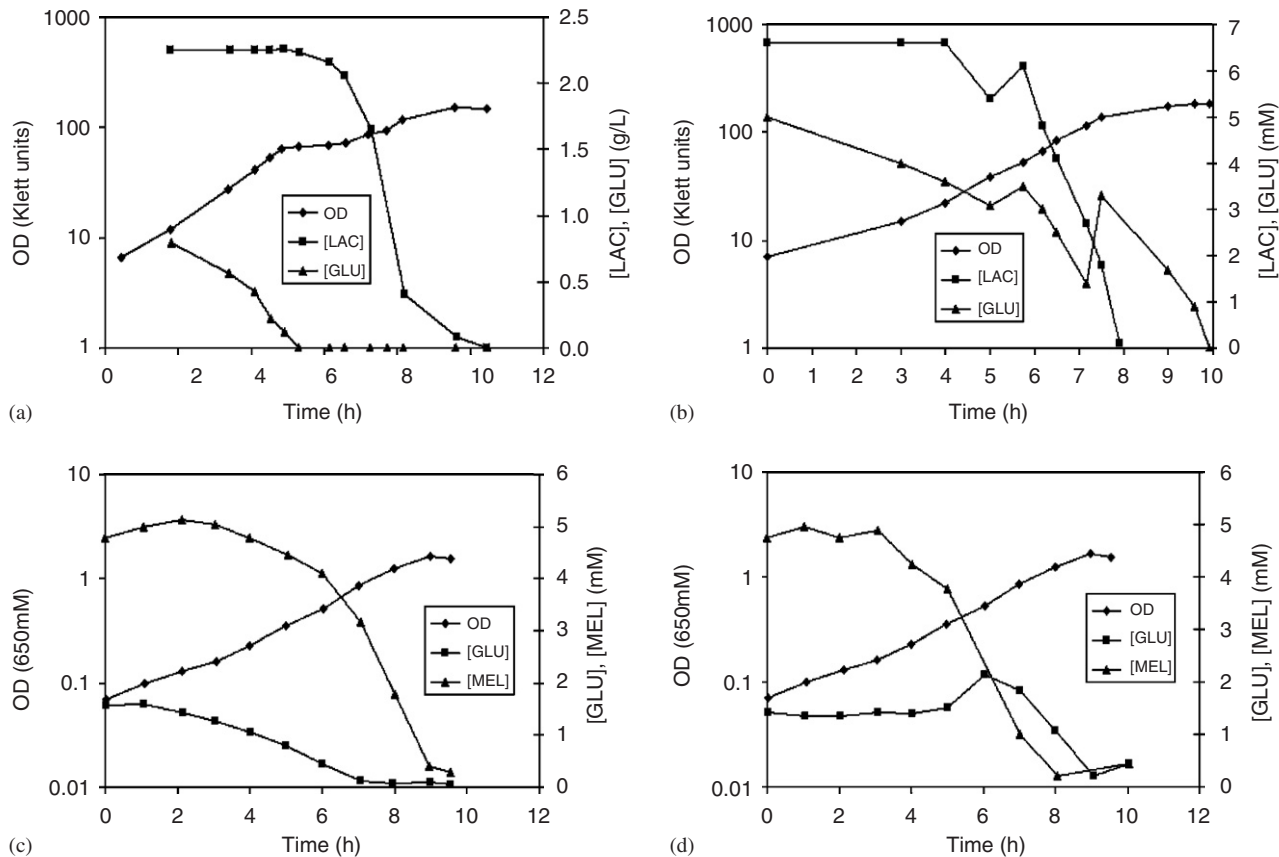
Fig. 13. Bistability in mixed-substrate growth: *Upper panel*: growth of *Streptococcus mutans* GS5 on a mixture of lactose (LAC) and glucose (GLU) (Liberman and Bleiweis, 1984). (a) Glucose is consumed preferentially if the cells are precultured on glucose. (b) Glucose and lactose are consumed simultaneously if the cells are precultured on lactose. *Lower panel*: growth of *Salmonella typhimurium* SB1476 on a mixture on a mixture of glucose (GLU) and melibiose (MEL) (Kuroda et al., 1992). (c) Glucose-precultured cells consume glucose before melibiose. (d) Melibiose-precultured cells consume melibiose before glucose. In (b) and (d), the concentration of glucose increases at $t \approx 8$ and $t \approx 6$ h, respectively. It is believed that is due to expulsion of the glucose produced from intracellular hydrolysis of lactose and melibiose, respectively.

4. Discussion

We have shown that a minimal model accounting for only enzyme induction and dilution captures and explains all the substrate consumption patterns observed in the experimental literature. In what follows, we discuss the robustness of the model, and its implications for the problem of size regulation in development.

4.1. Robustness of the model

Given the simplicity of the model, it is necessary ask whether the properties of the model will be preserved if additional metabolic details and regulatory mechanisms are incorporated in the model. Now, the defining property of the minimal model is that the enzymes follow competitive dynamics. We show below that this property is not a consequence of the particular kinetics assumed in the model. It is the outcome of two very general characteristics possessed by most systems of mixed-substrate growth.

To see this, it is useful to consider the generalized Lotka–Volterra model for competing species (Hirsch and Smale, 1974, Chapter 12). This model postulates that the competitive interactions between two species are captured by the relations

$$\frac{dN_i}{dt} = f_i(N_1, N_2), \quad f_1(0, N_2) = f_2(N_1, 0) = 0 \quad \text{and}$$

$$\frac{\partial f_1}{\partial N_2}, \frac{\partial f_2}{\partial N_1} < 0.$$

In other words, the essence of competitive interactions can be distilled into two properties:

(a) The growth of a species is impossible in the absence of that species ($dN_i/dt = 0$ whenever $N_i = 0$).
(b) Each species inhibits the growth of the other species ($\partial f_1/\partial N_2, \partial f_2/\partial N_1 < 0$).

These properties, by themselves, imply the existence of all the dynamics associated with competitive interactions, namely, the absence of limit cycles, and the existence of extinction and coexistence steady states.

Now, properties (a) and (b) will be manifested in most systems of mixed-substrate growth. Indeed, the evolution of the enzymes during the first exponential growth phase can be described by the relations

$$\frac{de_i}{dt} = g_i(e_1, e_2) \equiv r_{e,i}(e_1, e_2) - r_g(e_1, e_2)e_i.$$

If we assume that

(1) each enzyme is necessary for its own synthesis, i.e. $r_{e,i} = 0$ whenever $e_i = 0$,
(2) each enzyme has either no effect or inhibits the synthesis of the other enzyme, i.e. $\partial r_{e,1}/\partial e_2$, $\partial r_{e,2}/\partial e_1 \leqslant 0$,
(3) the specific growth rate is an increasing function of e_1 and e_2, i.e. $\partial r_g/\partial e_1$, $\partial r_g/\partial e_2 > 0$,

then the enzymes satisfy both the hypotheses of the generalized model for competing species: (a) There is no enzyme synthesis in the absence of the enzyme ($de_i/dt = 0$ whenever $e_i = 0$), and (b) each enzyme inhibits the synthesis of the other enzyme ($\partial g_1/\partial e_2$, $\partial g_2/\partial e_1 < 0$). Consequently, they will display extinction and coexistence dynamics.

It remains to consider the generality of Assumptions 1–3.

Assumption 1 will be satisfied whenever the substrates are transported by unique inducible enzymes. In these cases, the enzymes are required for the existence of the inducer ($e_i = 0 \Rightarrow x_i = 0$), and the inducers are necessary for the synthesis of the enzymes ($x_i = 0 \Rightarrow r_{e,i} = 0$); hence, $e_i = 0 \Rightarrow r_{e,i} = 0$. One can imagine two cases in which Assumption 1 is violated. First, if an enzyme is constitutive, it is synthesized even in the absence of the inducer ($x_i = 0 \nRightarrow r_{e,i} = 0$). Second, in the presence of a gratuitous inducer, such as IPTG, which can enter the cell even in the absence of lactose permease, the enzyme is not required for the existence of the inducer ($e_i = 0 \nRightarrow x_i = 0$). In both cases, the "extinction" steady state ceases to exist, and the

substrates will be consumed simultaneously. This is consistent with experiments (Fig. 14).

Assumption 2 will be satisfied provided the enzymes do not activate each other. But all the known regulatory mechanisms invariably entail direct or indirect inhibition of one of the enzymes by the other enzyme. This includes inducer exclusion (dephosphorylated enzyme II^{glc} inhibits lac permease), and cAMP activation (dephosphorylation of II^{glc} causes a reduction of cAMP levels, which in turn inhibits lac transcription).

Assumption 3 will be satisfied if the yield of biomass on a substrate during single-substrate growth does not change markedly during mixed-substrate growth. In the model, the yields were assumed to be constant. This is certainly true for conservative substrates since $Y_i = 1$. It is also observed to hold in many mixtures of carbon sources (Egli et al., 1982; Narang et al., 1997b). However, it is conceivable that there are systems in which the yields vary with the enzyme levels. In such cases, the specific growth rate will have the form, $r_g(e_1, e_2) = Y_1(e_1, e_2)V_{s,1}e_1 + Y_2(e_1, e_2)V_{s,2}e_2$. At present, the data is not sufficient for determining the extent to which the yields vary with the enzyme levels.

It is therefore clear that inclusion of various regulatory mechanisms will enhance the mutual inhibition due from dilution. However, the qualitative behavior will be preserved, since the enzymes will still follow Lotka–Volterra dynamics. Thus, the key property of the model, namely, competitive dynamics of the enzymes, is quite robust insofar as the perturbations with respect to regulatory mechanisms are concerned.

The notion that diauxic growth is the outcome of competitive interactions between the enzymes is not new. It can be found in the earliest papers on diauxic growth. In 1947, Monod noted that (Monod, 1947, p. 254)

"it appears that the mechanisms involved in diauxic inhibition have the character of *competitive interactions* between different specific enzyme-forming systems."
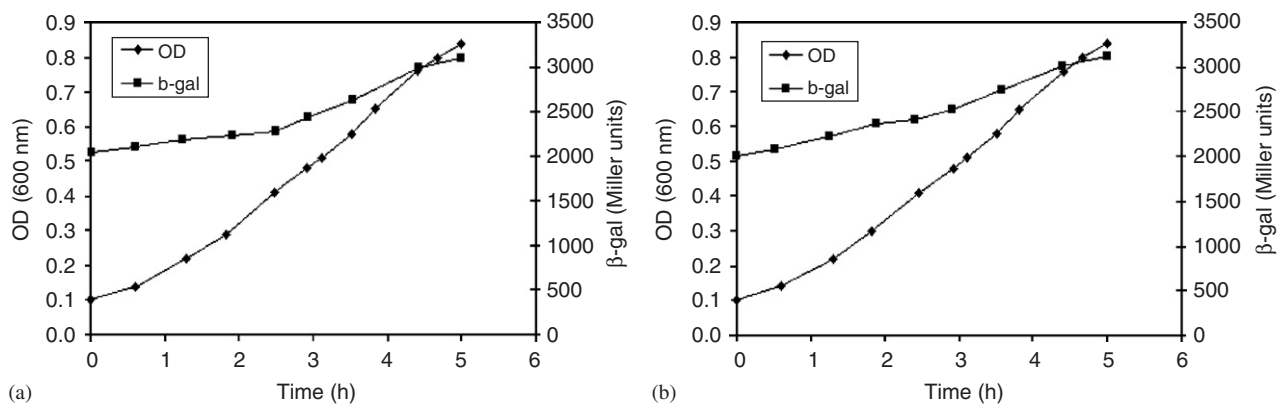

Fig. 14. Disappearance of the diauxie when the enzymes are not necessary for their own synthesis (Inada et al., 1996, Fig. 6.) Synthesis of β-galactosidase persists in the presence of glucose if (a) *lacI* is mutated so that *lac* transcription becomes constitutive or (b) IPTG is present in the medium. In the first case, *lac* transcription is constitutive, i.e. it persists even in the absence of the inducer. In the second case, *lac* transcription is no longer dependent on the existence of the permease.

He observed, furthermore, that the (Monod, 1947, p. 259).

"existence of competitive interactions in the synthesis of different specific enzymes appears to be a fact of fundamental significance in enzymatic adaptation, and one for which any conception of the phenomenon should be able to account."

However, these conclusions were based on the kinetics of the enzyme levels during diauxic growth, and had no mechanistic basis.

The above argument, first made in Narang (1998a), shows the mechanistic basis of the competitive interactions in a mathematically precise fashion.

4.2. Implication of the model for development

Diauxic growth has played a critical role in shaping models of patterning in development. The first link between genetics and development was established in the late 1940s by appealing to the following argument (Gilbert, 2002). During diauxic growth, cells possessing identical genes synthesize different proteins at distinct times (namely, the first and second exponential growth phases). By analogy, patterning in differentiation could be viewed as the synthesis of different proteins at distinct times and locations (Monod, 1947; Spiegelman, 1948). From this standpoint, diauxic growth and developmental patterning can be viewed as "temporal" and "spatiotemporal" differentiation, respectively.

The subsequent discovery of the molecular mechanisms involved in developmental patterning have confirmed the above hypothesis. It has been found that developmental patterns are generated by genetic switches similar in principle, but more complex in detail, than the genetic switch of the lac operon (Ptashne and Gann, 2002, Chapter 3).

Despite remarkable successes in developmental patterning, there are outstanding questions about *size regulation*, i.e. the mechanisms by which patterning is coupled to growth (Day and Lawrence, 2000; Hafen and Stocker, 2003; Serrano and O'Farrell, 1997). Examples of such questions include: what determines the size of organs and organisms, i.e. why does their growth cease at a certain time? and why is development *scale-invariant*, i.e. why is the size of the organs is proportional to the size of the organism?

The model presented here may be relevant to the problem of size regulation. It shows that the "temporal" differentiation in the diauxie is coupled to growth, and this coupling is mediated by the process of enzyme dilution. Inasmuch as the diauxie is a paradigm of the mechanisms controlling cellular differentiation, a similar mechanism may lie at the heart of the coupling between developmental patterning and growth. Based on the minimal model, one can speculate, for instance, that organ growth ceases at a certain time because growth-promoting enzymes are driven to "extinction" at sufficiently high growth rates.

The model also has implications for the problem of scale invariance. In many mathematical models of development, pattern formation occurs when a homogeneous steady state of a reaction–diffusion system

$$\frac{\partial c}{\partial t} = D\nabla^2 c - r(c, p), \tag{27}$$

becomes unstable due to the onset of a Turing instability (Murray, 1989). Here, $c(x, t)$ denotes the vector of morphogen concentrations, D is the matrix of diffusivities, and $r(c, p)$ is the reaction rate vector expressed as a function of c and a vector of parameters, p. In general, the patterns predicted by these models are not scale-invariant. However, this problem can be resolved if the system is fed more information about its size (say, L). For instance, perfect scale invariance is obtained if the diffusivities or rate constants are proportional to L^2, and plausible mechanisms for such a dependence have been proposed (Othmer and Pate, 1980; Ishihara and Kaneko, 2006).

In growing systems, however, information regarding the growth rate is constantly fed to the mechanism driving pattern formation. Indeed, in the presence of growth, Eq. (27) becomes

$$\frac{\partial c}{\partial t} + v.\nabla c = D\nabla^2 c - r(c, p) - c\nabla \cdot v, \tag{28}$$

where $v(x, t)$ is the velocity vector field, $v \cdot \nabla c$ is the accumulation of the morphogens due to convection, $\nabla \cdot v$ is the specific growth rate, and $c\nabla \cdot v$ is the dilution of the morphogens due to growth. Crampin et al. have shown that these equations exhibit a certain degree of scale invariance—as the system grows, the number of pattern elements remains the same despite a doubling of the system size (Crampin et al., 1999, 2002). Further analysis of this class of equations offers the promise of deeper insights into the coupling between patterning and growth.

5. Conclusions

(1) We showed that a minimal model accounting for enzyme induction and dilution, but not cAMP activation and inducer exclusion, captures and explains all the observed substrate consumption patterns, including diauxic growth, simultaneous consumption, and bistable growth. This suggests that the dynamics characteristic of mixed-substrate growth are already inherent in the minimal structure associated with induction and dilution. We find that many of the molecular mechanisms, such as inducer exclusion, serve to amplify these inherent dynamics.

(2) We constructed bifurcation diagrams showing the parameter values at which the various substrate consumption patterns will be observed. The bifurcation diagrams explain the phenotypic responses to various genetic perturbations, including lesions in the genes for the repressor, operator, and the transport enzymes.

Importantly, they provide a simple explanation for the "reversal of the diauxie," a phenomenon which is quite difficult to explain in terms of molecular mechanisms. The bifurcation diagrams also provide deep insights into the mechanisms underlying the empirically observed correlations between the substrate consumption patterns and the single-substrate growth rates. We found that

(a) when the induction kinetics are hyperbolic, the preferred substrate is always the one that supports a higher growth rate. This correlation is, therefore, unlikely to be the outcome of optimal design. It is a natural consequence of the fact that the enzymatic dynamics are governed by the rates of induction and dilution.

If induction is sigmoidal, it is possible for the preferred substrate to support a lower growth rate than the less preferred substrate. We presented experimental data illustrating this case.

(b) the existence of comparable growth rates is neither necessary nor sufficient for simultaneous consumption. When the saturation constants are small, simultaneous consumption occurs regardless of the maximum specific growth rates, since induction is quasiconstitutive. If the saturation constants are large, simultaneous consumption is impossible even if the growth rates are comparable.

(3) The key property of the model, namely, competitive dynamics of the enzymes, is quite robust with respect to structural perturbations.

(4) The model has implications for the problem of size regulation in development, since it provides a mechanism for coupling differentiation and growth, namely, protein dilution.
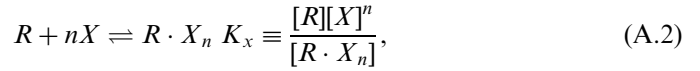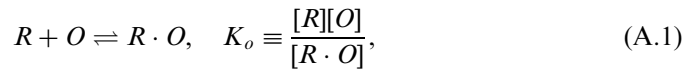
Acknowledgments

Appendix A. Interpretation of n_i, $V_{e,i}$, and $K_{e,i}$ in terms of molecular interactions

To express n_i, $V_{e,i}$, and $K_{e,i}$ in terms of molecular parameters, we appeal to the Yagil and Yagil model (Yagil and Yagil, 1971). For notational clarity, we shall ignore the subscript i for the substrate; thus, the operator, inducer, and repressor will be denoted by O, X, and R, respectively. Furthermore, their concentrations will be denoted $[O]$, $[X]$, and $[R]$, respectively.

The Yagil and Yagil model views induction as the outcome of a competition for the repressor between the operator and the inducer. Induction occurs when the inducer molecules sequester the repressors away from the operator. The competitive interactions are represented by two binding equilibria

$$R + O \rightleftharpoons R \cdot O, \quad K_o \equiv \frac{[R][O]}{[R \cdot O]}, \tag{A.1}$$

$$R + nX \rightleftharpoons R \cdot X_n \quad K_x \equiv \frac{[R][X]^n}{[R \cdot X_n]}, \tag{A.2}$$

where n denotes the number of inducer molecules that bind to 1 molecule of repressor; $[R \cdot O]$, $[R \cdot X_n]$ denote the concentrations of the complexes, $R \cdot O$, $R \cdot X_n$, respectively; and K_o, K_x denote the dissociation constants for the two equilibria.

It is assumed that

(1) enzyme synthesis is limited by the transcription rate, i.e. translation is not limiting. Thus, the specific enzyme synthesis rate is proportional to the specific transcription rate. Furthermore, the specific transcription rate is proportional to the concentration of the free operator, i.e.

$$r_e = v[O], \tag{A.3}$$

where v denotes the enzyme synthesis rate per unit mass of operator.

(2) the total concentrations of O and R, denoted $[O]_t$ and $[R]_t$, respectively, are conserved, i.e.

$$[O]_t = [O] + [R \cdot O], \tag{A.4}$$

$$[R]_t = [R] + [R \cdot O] + [R \cdot X_n]. \tag{A.5}$$

These two relations, together with Eqs. (A.1)–(A.2), constitute four equations in four unknowns, namely, $[O]$, $[R]$, $[R \cdot O]$, and $[R \cdot X_n]$. In principle, these equations can be solved for $[O]$, and substituted in (A.3) to obtain r_e. However, since the solution is cumbersome, it is convenient to make the following additional assumption.

(3) The repressor is bound primarily to the inducer (rather than the operator), i.e.

$$[R \cdot O] \ll [R]_t.$$

This assumption is valid under most conditions because the operator concentration (~ 2 per cell) is significantly smaller than the total repressor concentration (at least ~ 10 molecules per cell).

These assumptions yield

$$r_e = v[O] = V_e \frac{K_x + [X]^n}{K_x(1 + [R]_t/K_o) + [X]^n},$$

where $V_e \equiv v[O_t]$.

In the case of *constitutive* enzymes, the repressor has a weak affinity for the operator, i.e. $K_o \gg [R]_t$, so that

$$r_e \approx V_e$$

regardless of the inducer concentration.

In the case of *inducible* enzymes, the repressor has a high affinity for the operator, i.e. $K_o \ll [R]_t$, so that

$$r_e \approx V_e \frac{K_x + [X]^n}{K_x[R]_t/K_o + [X]^n}.$$

This is a monotonically increasing function of $[X]$ with a small non-zero intercept. Neglecting this small "basal" enzyme synthesis rate yields[8]

$$r_e \approx V_e \frac{[X]^n}{K_e^n + [X]^n}, \quad K_e^n \equiv \frac{K_x}{K_o}[R]_t.$$

Appendix B. Derivation of the equations

Eqs. (3)–(5) implicitly define the specific growth rate and the evolution of the cell density. To see this, observe that since all the intracellular concentrations are expressed as mass fractions (g/gdw), their sum equals 1, i.e. $x_1 + x_2 + e_1 + e_2 + c^- = 1$. Hence, addition of Eqs. (3)–(5) yields

$$0 = \sum_{i=1}^{2} r_{s,i} - \sum_{i=1}^{2} (1 - Y_i) r_{x,i} - \frac{1}{c} \frac{dc}{dt},$$

which can be rewritten in the more familiar form

$$\frac{dc}{dt} = r_g c, \quad r_g \equiv \sum_{i=1}^{2} r_{s,i} - \sum_{i=1}^{2} (1 - Y_i) r_{x,i},$$

where r_g denotes the specific growth rate.

We can simplify the model by observing that $x_i \sim 10^{-3}$ g/gdw (Chung and Stephanopoulos, 1996) and $r_{s,i}, r_{x,i} \sim 1$ g gdw^{-1} h^{-1}. Thus, x_i attains quasisteady state on a time scale of 10^{-3} h. Moreover, the dilution term $r_g x_i \sim 10^{-4}$ g gdw^{-1} h^{-1} is negligibly small compared to $r_{s,i}, r_{x,i}$. Hence, within a few seconds, (3) becomes, $0 \approx r_{s,i} - r_{x,i}$, which implies that $r_g \approx \sum_i Y_i r_{s,i}$, i.e. Y_i is essentially the yield of biomass on S_i. Thus, we arrive at the equations

$$\frac{dc}{dt} = (Y_1 r_{s,1} + Y_2 r_{s,2}) c,$$

$$\frac{ds_i}{dt} = -r_{s,i} c,$$

$$\frac{de_i}{dt} = r_{e,i} - (Y_1 r_{s,1} + Y_2 r_{s,2}) e_i,$$

$$x_i \approx \frac{V_{s,i} e_i s_i / (K_{s,i} + s_i)}{k_{x,i}},$$

$$c^- = 1 - x_1 - x_2 - e_1 - e_2,$$

where x_i is obtained by solving the quasisteady state relation, $r_{x,i} \approx r_{s,i}$.

<hr/>

[8]Recent evidence suggests that in the case of the *lac* operon, the cooperativity does not arise from the binding of two inducer molecules to a single repressor molecule. Instead, it might be due to the cooperative binding of a single repressor molecule to two operators (Oehler et al., 2006).

Appendix C. Stability analysis of case 1 ($n_1 = n_2 = 1$)

In this case, the steady states satisfy the equations

$$0 = \left(\frac{1}{\kappa_1 + \varepsilon_1} - \varepsilon_1 - \alpha \varepsilon_2 \right) \varepsilon_1,$$

$$0 = \left(\alpha \frac{1}{\kappa_2 + \varepsilon_2} - \varepsilon_1 - \alpha \varepsilon_2 \right) \varepsilon_2.$$

and the Jacobian at any $(\varepsilon_1, \varepsilon_2)$ is

$$J(\varepsilon_1, \varepsilon_2) = \begin{bmatrix} \dfrac{\kappa_1}{(\kappa_1 + \varepsilon_1)^2} - 2\varepsilon_1 - \alpha \varepsilon_2 & -\alpha \varepsilon_1 \\ -\varepsilon_2 & \dfrac{\alpha \kappa_2}{(\kappa_2 + \varepsilon_2)^2} - \varepsilon_1 - 2\alpha \varepsilon_2 \end{bmatrix}.$$

C.1. Trivial steady state

It is evident that E_{00} exists, regardless of the parameter values. It is always an unstable node since

$$J(E_{00}) = \begin{bmatrix} \dfrac{1}{\kappa_1} & 0 \\ 0 & \dfrac{1}{\kappa_2} \end{bmatrix}$$

which implies that both eigenvalues, $1/\kappa_1$ and $1/\kappa_2$, are positive.

C.2. Semitrivial steady states

The semitrivial steady state, E_{10}, always exists. It is unique and given by

$$\varepsilon_1 = \frac{-\kappa_1 + \sqrt{\kappa_1^2 + 4}}{2}, \quad \varepsilon_2 = 0.$$

Since $1/(\kappa_1 + \varepsilon_1) = \varepsilon_1$ at E_{10}, the Jacobian at this steady state is

$$\begin{bmatrix} \dfrac{\kappa_1 \varepsilon_1}{\kappa_1 + \varepsilon_1} - 2\varepsilon_1 & -\alpha \varepsilon_1 \\ 0 & \dfrac{\alpha}{\kappa_2} - \varepsilon_1 \end{bmatrix},$$

and the eigenvalues are

$$\lambda_1 = \frac{\kappa_1 \varepsilon_1}{\kappa_1 + \varepsilon_1} - 2\varepsilon_1 = -\varepsilon_1 \frac{\kappa_1 + 2\varepsilon_1}{\kappa_1 + \varepsilon_1} < 0, \quad \lambda_2 = \frac{\alpha}{\kappa_2} - \varepsilon_1.$$

Hence, E_{10} is stable (as a node) if and only if

$$\lambda_2 = \frac{\alpha}{\kappa_2} - \varepsilon_1 < 0 \Leftrightarrow \alpha < \kappa_2 \varepsilon_1|_{E_{10}} \Leftrightarrow \frac{\kappa_2}{\alpha} - \kappa_1 > \frac{\alpha}{\kappa_2}. \quad (C.1)$$

A similar analysis of the semitrivial steady state, E_{01}, shows that it always exists. It is unique and given by

$$\varepsilon_1 = 0, \quad \varepsilon_2 = \frac{-\kappa_2 + \sqrt{\kappa_2^2 + 4}}{2}.$$

It is stable (as a node) if and only if

$$\alpha > \frac{1}{\kappa_1 \varepsilon_2|_{E_{01}}} \quad \Leftrightarrow \quad \alpha(\alpha\kappa_1 - \kappa_2) > \frac{1}{\kappa_1}. \qquad (C.2)$$

C.3. Non-trivial steady state(s)

The non-trivial steady state(s), E_{11}, satisfy the equations

$$0 = \frac{1}{\kappa_1 + \varepsilon_1} - \varepsilon_1 - \alpha\varepsilon_2, \qquad (C.3)$$

$$0 = \alpha \frac{1}{\kappa_2 + \varepsilon_2} - \varepsilon_1 - \alpha\varepsilon_2. \qquad (C.4)$$

Eliminating ε_2 from these equations yields the equation

$$\frac{1}{\kappa_1 + \varepsilon_1} = (1 + \alpha^2)\varepsilon_1 + \alpha(\alpha\kappa_1 - \kappa_2),$$

which has at most 1 positive root, and it exists if and only if

$$\alpha(\alpha\kappa_1 - \kappa_2) < \frac{1}{\kappa_1} \quad \Leftrightarrow \quad E_{01} \quad \text{is unstable.}$$

On the other hand, eliminating ε_1 from (C.3)–(C.4) yields the equation

$$\frac{\alpha}{\kappa_2 + \varepsilon_2} = \left(\frac{1}{\alpha} + \alpha\right)\varepsilon_2 + \frac{\kappa_2}{\alpha} - \kappa_1$$

which has at most 1 positive root, and it exists if and only if

$$\frac{\kappa_2}{\alpha} - \kappa_1 < \frac{\alpha}{\kappa_2} \quad \Leftrightarrow \quad E_{10} \quad \text{is unstable.}$$

Thus, E_{11} exists if and only if both E_{10} and E_{01} are unstable. Furthermore, it is unique whenever it exists, and is given by

$$\varepsilon_1 = \frac{(\alpha\kappa_2 - \kappa_1) - 2\alpha^2\kappa_1 + \sqrt{(\alpha\kappa_2 - \kappa_1)^2 + 4[(1 + \alpha^2) + \alpha\kappa_2]}}{2(1 + \alpha^2)},$$

$$\varepsilon_2 = \frac{-\alpha(\alpha\kappa_2 - \kappa_1) - 2\kappa_2 + \sqrt{(\alpha\kappa_2 - \kappa_1)^2 + 4[(1 + \alpha^2) + \alpha\kappa_2]}}{2(1 + \alpha^2)}.$$

It turns out that E_{11} is stable whenever it exists since (C.3)–(C.4) imply that

$$J_{11} = \frac{\kappa_1}{(\kappa_1 + \varepsilon_1)^2} - 2\varepsilon_1 - \alpha\varepsilon_2 = -\frac{\varepsilon_1}{\kappa_1 + \varepsilon_1}(\kappa_1 + 2\varepsilon_1 + \alpha\varepsilon_2) < 0$$

and

$$J_{22} = \frac{\alpha\kappa_2}{(\kappa_2 + \varepsilon_2)^2} - \varepsilon_1 - 2\alpha\varepsilon_2 = -\frac{\varepsilon_2}{\kappa_2 + \varepsilon_2}(\alpha\kappa_2 + \varepsilon_1 + 2\alpha\varepsilon_2) < 0$$

so that $\operatorname{tr} J(E_{11}) < 0$ and

$$\det J(E_{11}) = (\kappa_1 + \alpha\kappa_2)\varepsilon_1 + \alpha(\kappa_1 + \alpha\kappa_2)\varepsilon_2 + 4\alpha\varepsilon_1\varepsilon_2 + 2\alpha^2\varepsilon_2^2 > 0.$$

Hence, the eigenvalues of $J(E_{11})$ have negative real parts.

We conclude that E_{11} exists if and only if

$$\text{Both } E_{10} \text{ and } E_{01} \text{ are unstable} \quad \Leftrightarrow \quad \frac{1}{\kappa_1 \varepsilon_2|_{E_{01}}} < \alpha < \kappa_2 \varepsilon_1|_{E_{10}}. \qquad (C.5)$$

Furthermore, it is unique and stable whenever it exists.

C.4. Disposition of the surfaces of α_*, α^*, and α_g

The surface of α_g lies between the surfaces of $\alpha_*(\kappa_1, \kappa_2)$ and $\alpha^*(\kappa_1, \kappa_2)$, i.e.

$$\alpha_*(\kappa_1, \kappa_2) < \alpha_g(\kappa_1, \kappa_2) < \alpha^*(\kappa_1, \kappa_2) \qquad (C.6)$$

for all $\kappa_1, \kappa_2 > 0$. To see this, observe that

$$\left(\frac{1}{x} + \frac{x}{2}\right)^2 > 1 + \frac{x^2}{4} \Rightarrow \frac{-x + \sqrt{x^2 + 4}}{2} < \frac{1}{x}$$

for all $x > 0$. Hence

$$\frac{-\kappa_1 + \sqrt{\kappa_1^2 + 4}}{2/\kappa_2} < \frac{-\kappa_1 + \sqrt{\kappa_1^2 + 4}}{-\kappa_2 + \sqrt{\kappa_2^2 + 4}} < \frac{2/\kappa_1}{-\kappa_2 + \sqrt{\kappa_2^2 + 4}}$$

for all $\kappa_1, \kappa_2 > 0$, and (C.6) follows immediately from the definitions of α_*, α^*, and α_g.

Appendix D. Stability analysis of case 2 ($n_1 = 2$, $n_2 = 1$)

In this case, the steady states satisfy the equations

$$0 = \left(\frac{\varepsilon_1}{\kappa_1^2 + \varepsilon_1^2} - \varepsilon_1 - \alpha\varepsilon_2\right)\varepsilon_1,$$

$$0 = \left(\alpha \frac{1}{\kappa_2 + \varepsilon_2} - \varepsilon_1 - \alpha\varepsilon_2\right)\varepsilon_2.$$

and the Jacobian at any $(\varepsilon_1, \varepsilon_2)$ is

$$J(\varepsilon_1, \varepsilon_2) = \begin{bmatrix} \dfrac{2\kappa_1^2\varepsilon_1}{(\kappa_1^2 + \varepsilon_1^2)^2} - 2\varepsilon_1 - \alpha\varepsilon_2 & -\alpha\varepsilon_1 \\[2mm] -\varepsilon_2 & \dfrac{\alpha\kappa_2}{(\kappa_2 + \varepsilon_2)^2} - \varepsilon_1 - 2\alpha\varepsilon_2 \end{bmatrix}.$$

In what follows, we study the conditions on the parameter values for the existence and stability of all four types of steady states.

D.1. Trivial steady state

The trivial steady, E_{00}, always exists, regardless of the parameter values. The Jacobian is singular at this steady state, but we can infer its stability from the dynamics on the invariant lines, $\varepsilon_1 = 0$ and $\varepsilon_2 = 0$. Indeed, in the neighborhood of E_{00},

$$\left.\frac{d\varepsilon_1}{dt}\right|_{\varepsilon_2 = 0} \approx \varepsilon_1^2\left(\frac{1}{\kappa_1^2} - 1\right), \quad \left.\frac{d\varepsilon_2}{dt}\right|_{\varepsilon_1 = 0} \approx \frac{\alpha}{\kappa_2}\varepsilon_2 > 0.$$

Hence, E_{00} is a non-hyperbolic saddle if $\kappa_1 < 1$ and a non-hyperbolic unstable node if $\kappa_1 > 1$.

D.2. Semitrivial steady states

The semitrivial steady state, E_{10}, exists provided $\kappa_1 < 1$, in which case it is unique, and given by

$$\varepsilon_1 = \sqrt{1 - \kappa_1^2}, \quad \varepsilon_2 = 0.$$

Since $\varepsilon_1^2 + \kappa_{e,1}^2 = 1$ at this steady state, the Jacobian is

$$\begin{bmatrix} 2(\kappa_1^2 - 1)\varepsilon_1 & -\alpha\varepsilon_1 \\ 0 & \dfrac{\alpha}{\kappa_2} - \varepsilon_1 \end{bmatrix},$$

and the eigenvalues are

$$\lambda_1 = 2(\kappa_1^2 - 1)\varepsilon_1 < 0, \quad \lambda_2 = \frac{\alpha}{\kappa_2} - \varepsilon_1.$$

Hence, E_{10} is stable (as a node) if and only if

$$\lambda_2 = \frac{\alpha}{\kappa_2} - \varepsilon_1 |_{E_{10}} < 0 \iff \alpha < \kappa_2 \sqrt{1 - \kappa_1^2}. \tag{D.1}$$

Analysis of the steady state, E_{01}, shows that this steady state always exists, and is given by

$$\varepsilon_1 = 0, \quad \varepsilon_2 = \frac{-\kappa_2 + \sqrt{\kappa_2^2 + 4}}{2}.$$

The Jacobian at this steady state is

$$\begin{bmatrix} -\alpha\varepsilon_2 & 0 \\ -\varepsilon_2 & \dfrac{\alpha\kappa_2\varepsilon_2}{\kappa_2 + \varepsilon_2} - 2\alpha\varepsilon_2 \end{bmatrix},$$

and the eigenvalues are

$$\lambda_1 = -\alpha\varepsilon_2 < 0, \quad \lambda_2 = -\alpha\varepsilon_2 \frac{\kappa_2 + 2\varepsilon_2}{\kappa_2 + \varepsilon_2} < 0. \tag{D.2}$$

We conclude that E_{01} always exists and is stable (as a node).

D.3. Non-trivial steady state(s)

D.3.1. Existence

The non-trivial steady states satisfy the equations

$$0 = \frac{\varepsilon_1}{\kappa_1^2 + \varepsilon_1^2} - \varepsilon_1 - \alpha\varepsilon_2, \tag{D.3}$$

$$0 = \alpha \frac{1}{\kappa_2 + \varepsilon_2} - \varepsilon_1 - \alpha\varepsilon_2. \tag{D.4}$$

If $\kappa_1 > 0$, there are no non-trivial steady states, since (D.3) cannot be satisfied for any $\varepsilon_1, \varepsilon_2 > 0$. Indeed,

$$\kappa_1 > 1 \Rightarrow \frac{\varepsilon_1}{\kappa_1^2 + \varepsilon_1^2} - \varepsilon_1 - \alpha\varepsilon_2 = \varepsilon_1 \left(\frac{1}{\kappa_1^2 + \varepsilon_1^2} - 1 \right) - \alpha\varepsilon_2 < 0$$

for all $\varepsilon_1, \varepsilon_2 > 0$. Henceforth, we shall assume that $0 < \kappa_1 < 1$ and $\kappa_2 > 0$.

We begin by introducing a change of coordinates that reduces the problem to the existence of roots on a finite interval. Letting $\varepsilon_2 = v\varepsilon_1$, we rewrite the above system as

$$\frac{1}{\kappa_1^2 + \varepsilon_1^2} = 1 + \alpha v,$$

$$\frac{\alpha}{\kappa_2 + v\varepsilon_1} = \varepsilon_1(1 + \alpha v).$$

Solving the first equation for ε_1, and rewriting the second equation, we obtain

$$\varepsilon_1 = \sqrt{\frac{1}{1 + \alpha v} - \kappa_1^2},$$

$$\frac{\alpha}{1 + v\alpha} = v\varepsilon_1^2 + \kappa_2\varepsilon_1.$$

Hence, we obtain the following equation for v:

$$\frac{\alpha}{1 + v\alpha} = v \left(\frac{1}{1 + \alpha v} - \kappa_1^2 \right) + \kappa_2 \sqrt{\frac{1}{1 + \alpha v} - \kappa_1^2}.$$

Multiplying through by $(1 + \alpha v)$, we obtain

$$\alpha = v[1 - \kappa_1^2(1 + \alpha v)] + \kappa_2 \sqrt{(1 + \alpha v)[1 - \kappa_1^2(1 + \alpha v)]}.$$

Finally, we let

$$z = \kappa_1^2(1 + \alpha v), \quad v = \frac{1}{\alpha} \left(\frac{z}{\kappa_1^2} - 1 \right),$$

and rewrite the above equation as

$$1 = \frac{1}{\alpha^2 \kappa_1^2}(z - \kappa_1^2)(1 - z) + \frac{\kappa_2}{\alpha\kappa_1} \sqrt{z(1 - z)} = f(z, \alpha). \tag{D.5}$$

Observe that z uniquely determines v, and hence both ε_1 and ε_2. To ensure that both $\varepsilon_i > 0$, z must belong to the interval $(\kappa_1^2, 1)$. Thus, the problem is reduced to the existence of roots of (D.5) on the finite interval $(\kappa_1^2, 1)$.

Several properties of f are immediate:

$$f(1, \alpha) = 0 < 1, \quad f(\kappa_1^2, \alpha) = \frac{\kappa_2 \sqrt{1 - \kappa_1^2}}{\alpha},$$

and

$$f_{zz}(z, \alpha) = -\frac{2}{\alpha^2 \kappa_1^2} - \frac{\kappa_2[4z(1 - z) + (1 - 2z)^2]}{4\alpha\kappa_1[z(1 - z)]^{3/2}} < 0 \quad \forall \, 0 < z < 1,$$

so that $f(z, \alpha)$ is strictly concave down in z for each $\alpha > 0$ and for all $\kappa_1^2 < z < 1$. In particular, this implies that (D.5) has a unique root $z \in [\kappa_1^2, 1]$ if $f(\kappa_1^2, \alpha) > 1$, and at most two roots if $f(\kappa_1^2, \alpha) \leqslant 1$. Furthermore, we observe that $f_z(z, \alpha) \to -\infty$ as $z \to 1$,

$$f_z(\kappa_1^2, \alpha) = \frac{2(1 - \kappa_1^2)^{3/2} + \alpha\kappa_2(1 - 2\kappa_1^2)}{2\alpha^2\kappa_1^2 \sqrt{1 - \kappa_1^2}},$$

and

$$f_z(\kappa_1^2, \alpha_*) = \frac{2(1 - \kappa_1^2) + \kappa_2^2(1 - 2\kappa_1^2)}{2\kappa_1^2\kappa_2^2(1 - \kappa_1^2)}.$$

Hence, $f_z(\kappa_1^2, \alpha_*) > 0$ if and only if $2(1 - \kappa_1^2) + \kappa_2^2(1 - 2\kappa_1^2) > 0$, i.e.

$$\kappa_1 < \beta \equiv \sqrt{\frac{1 + \kappa_2^2}{2(1 + \kappa_2^2)}}.$$

Finally, we observe that $f(z, \alpha)$ decreases in α for each fixed z, and $f(z, \alpha) \to 0$ as $\alpha \to +\infty$.

We conclude that there are two scenarios:

(1) If $\kappa_1 < \beta$, then there exists $\alpha^* > \alpha_*$ such that (D.5) has only one root in $(\kappa_1^2, 1)$ for all $\alpha < \alpha_*$, two distinct roots in $(\kappa_1^2, 1)$ for all $\alpha_* < \alpha < \alpha^*$, and no roots for $\alpha > \alpha^*$. When $\alpha = \alpha_*$, (D.5) has two roots: $z = \kappa_1^2$ and another root in $(\kappa_1^2, 1)$. When $\alpha = \alpha^*$, (D.5) admits a double root in $(\kappa_1^2, 1)$.
(2) If $\kappa_1 \geqslant \beta$, then (D.5) admits only one root in $(\kappa_1^2, 1)$ for all $\alpha < \alpha_*$, and no roots for $\alpha > \alpha_*$. A single root $z = \kappa_1^2$ occurs if and only if $\alpha = \alpha_*$.

Thus, we obtain the bifurcation diagram shown in Fig. 11.

D.3.2. Computation of $\alpha^*(\kappa_1, \kappa_2)$

We have shown above that α^* exists for all $\kappa_1 < \beta$. Here, we present an algorithm for computing α^*, which rests upon the fact that the non-trivial nullclines for ε_1 and ε_2 touch at $\alpha = \alpha^*$.

Eliminating ε_2 from (D.3)–(D.4) yields the quartic polynomial

$$\varepsilon_1^4 \cdot (1 + \alpha^2) - \varepsilon_2^3 \cdot \alpha\kappa_2 + \varepsilon_1^2 \cdot [2\alpha^2\kappa_1^2 - (1 - \kappa_1^2)]$$
$$+ \varepsilon_1 \cdot \alpha\kappa_1^2 + \alpha^2\kappa_1^4 = 0. \qquad (D.6)$$

This equation has two equal real roots if and only if the discriminant is zero (Dickson, 1914, p. 41), i.e.

$$\triangle \equiv \frac{\alpha^2}{(1 + \alpha^2)^6}[c_0(\alpha^2)^3 + c_1(\alpha^2)^2 + c_2(\alpha^2) + c_3] = 0, \qquad (D.7)$$

where

$$c_0 = \kappa_1^8(4 + \kappa_2^2)^2 > 0,$$

$$c_1 = \frac{\kappa_1^6}{4}[8\kappa_1^4(\kappa_2^2 - 4) - (\kappa_2^2 + 2)(\kappa_2^2 + 4)^2 - 4\kappa_1^2(\kappa_2^2 + 4)(\kappa_2^2 + 8)],$$

$$c_2 = \frac{\kappa_1^4}{16}[16\kappa_1^8 + 32\kappa_1^6(\kappa_2^2 - 6) + (\kappa_2^2 + 4)^2$$
$$- 4\kappa_1^2(\kappa_2^2 + 4)(5\kappa_2^2 + 12)8\kappa_1^4(\kappa_2^4 - 11\kappa_2^2 - 44)],$$

$$c_3 = \frac{\kappa_1^4}{4}(1 - \kappa_1^2)^3[4(1 - \kappa_1^2) + \kappa_2^2] > 0.$$

For every $\kappa_1, \kappa_2 > 0$, Eq. (D.7) has three non-zero roots. One of these roots is negative since c_0 and c_3 are positive. Computations show that the remaining two roots are also positive. However, the nullclines touch in the first quadrant, $\varepsilon_1, \varepsilon_2 > 0$, only if $\kappa_1 < \beta$, and α is the largest

positive root. Thus, $\alpha^*(\kappa_1, \kappa_2)$ is the largest of the three roots of (D.7).

D.3.3. Stability

The stability of the steady states follows from the geometry of the non-trivial nullclines for ε_1 and ε_2. Indeed, it is known from the theory of the generalized Lotka–Volterra model for competing species that a non-trivial steady state is stable if and only if in the neighborhood of the non-trivial steady state, the non-trivial nullclines for both ε_1 and ε_2 have negative slopes, but the slope of the non-trivial nullcline for ε_2 is more negative (i.e. higher in absolute value) than the slope of the non-trivial nullcline for ε_1 (Hirsch and Smale, 1974, Chapter 12).

References

Asensio, C., Avigad, G., Horecker, B.L., 1963. Preferential galactose utilization in a mutant strain of E. coli.. Arch. Biochem. Biophys. 103, 299–309.

Brandt, B.W., Kelpin, F.D.L., van Leuwen, I.M.M., Kooijman, S.A.L.M., 2004. Modelling microbial adaptation to changing availability of substrates. Water Res. 38, 1004–1013.

Chung, J.D., Stephanopoulos, G., 1996. On physiological multiplicity and population heterogeneity of biological systems. Chem. Eng. Sci. 51, 1509–1521.

Clark, B., Holms, W.H., 1976. Control of the sequential utilization of glucose and fructose by Escherichia coli. J. Gen. Microbiol. 95, 191–201.

Cohn, M., Horibata, K., 1959. Inhibition by glucose of the induced synthesis of the β-galactoside-enzyme system of Escherichia coli. Analysis of maintenance. J. Bacteriol. 78, 601–612.

Crampin, E.J., Gaffney, E.A., Maini, P.K., 1999. Reaction and diffusion on growing domains: scenarios for robust pattern formation. Bull. Math. Biol. 61, 1093–1120.

Crampin, E.J., Hackborn, W.W., Maini, P.K., 2002. Pattern formation in reaction–diffusion models with nonuniform domain growth. Bull. Math. Biol. 64 (4), 747–769.

Daughton, C.G., Cook, A.M., Alexander, M., 1979. Phosphate and soil binding: factors limiting bacterial degradation of ionic phosphorus-containing pesticide metabolites. Appl. Environ. Microbiol. 37 (3), 605–609.

Day, S.J., Lawrence, P.A., 2000. Measuring dimensions: the regulation of size and shape. Development 127 (14), 2977–2987.

Dickson, L.E., 1914. Elementary Theory of Equations, first ed. Edition. Elementary Theory of Equations.

Egli, T., 1995. The ecological and physiological significance of the growth of heterotrophic microorganisms with mixtures of substrates. Adv. Microbiol. Ecol. 14, 305–386.

Egli, T., Käppeli, O., Fiechter, A., 1982. Regulatory flexibility of methylotrophic yeasts in chemostat culture: Simultaneous assimilation of glucose and methanol at a fixed dilution rate. Arch. Microbiol. 131, 1–7.

Gilbert, S.F., 2002. Enzymatic adaptation and the entrance of molecular biology into embryology. In: Sarkar, S. (Ed.), The Biology and History of Molecular Biology: New Perspectives. Boston Studies in the Philosophy of Science, Springer, Berlin.

Hafen, E., Stocker, H., 2003. How are the sizes of cells, organs, and bodies controlled? PLoS Biol. 1 (3), E86.

Hamilton, W.A., Dawes, E.A., 1959. A diauxic effect with Pseudomonas aeruginosa. Biochem. J. 71, 25P–26P.

Hamilton, W.A., Dawes, E.A., 1960. The nature of the diauxic effect with glucose and organic acids in Pseudomonas aeruginosa. Biochem. J. 76, 70P.

Hamilton, W.A., Dawes, E.A., 1961. Further observations on the nature of the diauxic effect with *Pseudomonas aeruginosa*. Biochem. J. 79, 25P.

Harder, W., Dijkhuizen, L., 1976. Mixed substrate utilization. In: Dean, A.C.R., Ellwood, D.C., Evans, C.G.T., Melling, J. (Eds.), Continuous Culture 6: Applications and New Fields. Ellis Horwood, Chichester, pp. 297–314 (Chapter 23).

Harder, W., Dijkhuizen, L., 1982. Strategies of mixed substrate utilization in microorganisms. Philos. Trans. R. Soc. London B 297, 459–480.

Hirsch, M.W., Smale, S., 1974. Differential Equations, Dynamical Systems, and Linear Algebra. Academic Press, New York (Chapter 12).

Inada, T., Kimata, K., Aiba, H., 1996. Mechanism responsible for the glucose-lactose diauxie in *Escherichia coli*: challenge to the cAMP model. Genes Cells 1, 293–301.

Ishihara, S., Kaneko, K., 2006. Turing pattern with proportion preservation. J. Theor. Biol. 238 (3), 683–693.

Jacob, F., Monod, J., 1961. Genetic regulatory mechanisms in the synthesis of proteins. J. Mol. Biol. 3, 318–356.

Joseph, E., Danchin, A., Ullmann, A., 1981. Regulation of galactose operon expression: glucose effects and role of cyclic adenosine 3',5'-monophosphate. J. Bacteriol. 146 (1), 149–154.

Kamogawa, A., Kurahashi, K., 1967. Inhibitory effect of glucose on the growth of a mutant strain of *Escherichia coli* defective in glucose transport system. J. Biochem. (Tokyo) 61 (2), 220–230.

Kimata, K., Takahashi, H., Inada, T., Postma, P., Aiba, H., 1997. cAMP receptor protein-cAMP plays a crucial role in glucose–lactose diauxie by activating the major glucose transporter gene in *Escherichia coli*. Proc. Natl Acad. Sci. USA 94, 12914–12919.

Kompala, D.S., Ramkrishna, D., Jansen, N.B., Tsao, G.T., 1986. Investigation of bacterial growth on mixed substrates: Experimental evaluation of cybernetic models. Biotechnol. Bioeng. 28, 1044–1055.

Kovarova-Kovar, K., Egli, T., 1998. Growth kinetics of suspended microbial cells: From single-substrate-controlled growth to mixed-substrate kinetics. Microbiol. Mol. Biol. Rev. 62, 646–666.

Kremling, A., Bettenbrock, K., Laube, B., Jahreis, K., Lengeler, J.W., Gilles, E.D., 2001. The organization of metabolic reaction networks. III. Application for diauxic growth on glucose and lactose. Metab. Eng. 3 (4), 362–379.

Kuroda, M., Osaki, N., Tsuda, M., Tsuchiya, T., 1992. Preferential utilization of glucose over melibiose, and vice versa in a PTS mutant of *Salmonella typhimurium*. Chem. Pharm. Bull. (Tokyo) 40 (6), 1637–1640.

Lee, I.H., Fredrickson, A.G., Tsuchiya, H.M., 1974. Diauxic growth of *Propionibacterium shermanii*. Appl. Microbiol. 28, 831–835.

Lengeler, J., Lin, E.C., 1972. Reversal of the mannitol–sorbitol diauxie in *Escherichia coli*. J. Bacteriol. 112 (2), 840–848.

Liberman, E.S., Bleiweis, A.S., 1984. Role of the phosphoenolpyruvate-dependent glucose phosphotransferase system of *Streptococcus mutans* GS5 in the regulation of lactose uptake. Infect. Immun. 43 (2), 536–542.

Liu, P.H., Svoronos, S.A., Koopman, B., 1998. Experimental and modeling study of diauxic lag of *Pseudomonas denitrificans* switching from oxic to anoxic conditions. Biotechnol. Bioeng. 60 (6), 649–655.

Mahadevan, R., Edwards, J.S., Doyle, F.J., 2002. Dynamic flux balance analysis of diauxic growth in *Escherichia coli*. Biophys. J. 83 (3), 1331–1340.

Monod, J., 1942. Recherches sur la croissance des cultures bactériennes (Studies on the growth of bacterial cultures). Actua. Sci. Ind. 911, 1–215.

Monod, J., 1947. The phenomenon of enzymatic adaptation and its bearings on problems of genetics and cellular differentiation. Growth 11, 223–289.

Murray, J.D., 1989. Mathematical Biology. Biomathematics Texts. Springer, New York.

Narang, A., 1998a. The dynamical analogy between microbial growth on mixtures of substrates and population growth of competing species. Biotechnol. Bioeng. 59, 116–121.

Narang, A., 1998b. The steady states of microbial growth on mixtures of substitutable substrates in a chemostat. J. Theor. Biol. 190, 241–261.

Narang, A., 2006. Comparitive analysis of some models of gene regulation in mixed-substrate microbial growth, J Theor. Biol. 242, 489–501.

Narang, A., Konopka, A., Ramkrishna, D., 1997a. The dynamics of microbial growth on mixtures of substrates in batch reactors. J. Theor. Biol. 184, 301–317.

Narang, A., Konopka, A., Ramkrishna, D., 1997b. New patterns of mixed substrate growth in batch cultures of *Escherichia coli* K12. Biotechnol. Bioeng. 55, 747–757.

Neidhardt, F.C., Magasanik, B., 1957. Reversal of the glucose inhibition of histidase biosynthesis in *Aerobacter aerogenes*. J. Bacteriol. 73 (2), 253–259.

Notley-McRobb, L., Death, A., Ferenci, T., 1997. The relationship between external glucose concentration and cAMP levels inside *Escherichia coli*: implications for models of phosphotransferase-mediated regulation of adenylate cyclase. Microbiology 143 (Pt 6), 1909–1918.

Oehler, S., Alberti, S., Müller-Hill, B., 2006. Induction of the lac promoter in the absence of DNA loops and the stoichiometry of induction. Nucleic Acids Res. 34 (2), 606–612.

Okada, T., Ueyama, K., Niiya, S., Kanazawa, H., Futai, M., Tsuchiya, T., 1981. Role of inducer exclusion in preferential utilization of glucose over melibiose in diauxic growth of *Escherichia coli*. J. Bacteriol. 146 (3), 1030–1037.

Othmer, H.G., Pate, E., 1980. Scale-invariance in reaction-diffusion models of spatial pattern formation. Proc. Natl Acad. Sci. USA 77 (7), 4180–4184.

Panikov, N.S., 1995. Microbial Growth Kinetics. Chapman & Hall, London, p. 181, (Chapter 3).

Plumbridge, J., 2003. Regulation of gene expression in the PTS in *Escherichia coli*: The role and interactions of Mlc. Curr. Opin. Microbiol. 5, 187–193.

Postma, P.W., Lengeler, J.W., Jacobson, G.R., 1993. Phosphoenolpyruvate: carbohydrate phosphotransferase systems of bacteria. Microbiol. Rev. 57 (3), 543–594.

Ptashne, M., Gann, A., 2002. Genes & Signals. Cold Spring Harbor Laboratory Press, Cold Spring Harbor, New York.

Ramakrishna, R., Ramkrishna, D., Konopka, A., 1996. Cybernetic modeling of growth in mixed, substitutable substrate environments: Preferential and simultaneous utilization. Biotechnol. Bioeng. 52, 141–151.

Roseman, S., Meadow, N.D., 1990. Signal transduction by the bacterial phosphotransferase system Diauxie and the *crr* gene (J Monod revisited). J. Biol. Chem. 265 (6), 2993–2996.

Santillan, M., Mackey, M.C., 2004. Influence of catabolite repression and inducer exclusion on the bistable behavior of the *lac* operon. Biophys. J. 86 (3), 1282–1292.

Serrano, N., O'Farrell, P.H., 1997. Limb morphogenesis: connections between patterning and growth. Curr. Biol. 7 (3), R186–R195.

Spiegelman, S., 1948. Differentiation as the controlled production of unique enzymatic patterns. In: Danielli, J.F., Brown, R. (Eds.), Growth in relation to differentiation and morphogenesis. In Symposium of the Society for Experimental Biology. No. II. Academic Press, New York, pp. 286–325.

Tanaka, S., Fraenkel, D.G., Lin, E.C., 1967. The enzymatic lesion of strain MM-6, a pleiotropic carbohydrate-negative mutant of *Escherichia coli*. Biochem. Biophys. Res. Commun. 27 (1), 63–67.

Thattai, M., Shraiman, B.I., 2003. Metabolic switching in the sugar phosphotransferase system of *Escherichia coli*. Biophys. J. 85 (2), 744–754.

van Dedem, G., Moo-Young, M., 1973. Cell growth and extracellular enzyme synthesis in fermentations. Biotechnol. Bioeng. 15, 419–439.

Wong, P., Gladney, S., Keasling, J.D., 1997. Mathematical model of the *lac* operon: inducer exclusion, catabolite repression, and diauxic growth on glucose and lactose. Biotechnol. Prog. 13 (2), 132–143.

Yagil, G., Yagil, E., 1971. On the relation between effector concentration and the rate of induced enzyme synthesis. Biophys. J. 11, 11–17.